Geologica Acta, Vol.1, Nº3, 2003, 239-259
Available online at www.geologica-acta.com

geologica acta

# From thrust tectonics to diapirism. The role of evaporites in the kinematic evolution of the eastern South Pyrenean front

**M. SANS**

**Dept. Geodinàmica i Geofísica, Universitat de Barcelona**
Zona Universitària de Pedralbes, 08028 Barcelona. Spain. E-mail: sansicia@eic.ictnet.es

**ABSTRACT**

The South Pyrenean foreland has a buried thrust front geometry where evaporitic levels are present at the subsurface and are suitable to be detachment horizons. The thrust wedge geometry developed at the externalmost limit of the evaporitic levels permits to define the South Pyrenean Triangle zone. This triangle zone is an excellent scenario to study the influence of evaporitic layers in the thrust front geometry of a fold and thrust system and in the development of thrust wedges. Analogue modelling shows different thrust wedge geometries through the deformation history in relation to the different rheological properties of the detachment horizons. Presence of strain markers in the field permitted to quantify strain in the overburden. In addition, the possibility to access to the detachment at different locations permited the comparison between the deformation in the overburden and in the detachment horizon from the most frontal structures to the hinter ones. The structure in the detachment horizons are well preserved because the evaporitic levels are layered and because bulk shortening is small. Finally, analogue modelling of the development of a diapir near the crest of an anticline suggested a new hypothesis of the formation of diapirs in areas that have undergone compression.

*KEYWORDS* | **Salt tectonics. Southern Pyrenees. Diapirism. Fold-and-thrust belts. Analogue modelling.**

## INTRODUCTION

Salt tectonics deals with any tectonic deformation involving salt, or other evaporites, as a substratum or source layer, including halokinesis (Jackson and Talbot, 1991). It embraces a wide range of tectonic settings, influences basin dynamics and it is related to many economic activities such as oil exploration, mining and waste repositories.

Salt tectonics has been treated extensively in the literature, especially diapirism in extensional tectonic settings (Braunstein and O'Brien, 1968; Jeyon, 1986; Lerche and O'Brien, 1987; Cobbold, 1993; Jackson and Vendeville, 1994; Jackson et al., 1995; Davison et al., 1996; Vendeville et al., 2000). The reason may be that research in extensional salt tectonics is linked to the development of salt structures like pillows, diapirs, salt rollers, rafts or allochtonous salt sheets which generate important oil traps (Gulf of Mexico, Angola, Brazil, Caspian Sea and North Sea). Moreover salt diapirs of the main salt minning regions are mainly triggered by extension (e.g. Zechtein diapirs in Germany). In contrast, salt tectonics in compressional settings has been mainly approached from the regional point of view, focussing on the role of salt levels as decollement in the fold-and-thrust belts (Davis and Engelder, 1985; Letouzey et al., 1995). In spite of this, the geometry and evolution of the deformation front in relation to the presence of a ductile salt detachment has not been well documented. More recently, detachment folds have been studied from the theoretical point of view (Wiltschko

and Chapple, 1977; Dalhstrom, 1990; Epard and Groshong, 1993; Groshong and Epard 1994; Homza and Wallace, 1995; Hardy and Poblet, 1994; Poblet and McClay, 1996). However, the internal structure of the detachment horizons has not been explored in detail, and the attention given to the evolution of fish-tail structures, pop-ups, structures that sink into the ductile layer, their evolution in 3D and the role of multiple ductile detachments has not been sufficient. Moreover, many diapiric areas of the world have also undergone shortening, therefore the comprehension of the behavior of the salt levels during shortening is a clue for understanding polyphase deformation in salt areas.

Some of these topics are addressed here in order to improve the general knowledge and understanding of salt tectonics in compressional settings. The southern Pyrenean foreland was selected as study area because several Eocene salt horizons actted as the detachment levels for the foreland structures (Fig. 1); one of these horizons (Cardona Fm.) was accessible in different locations via underground salt mines; the salt is thinly bedded with clay

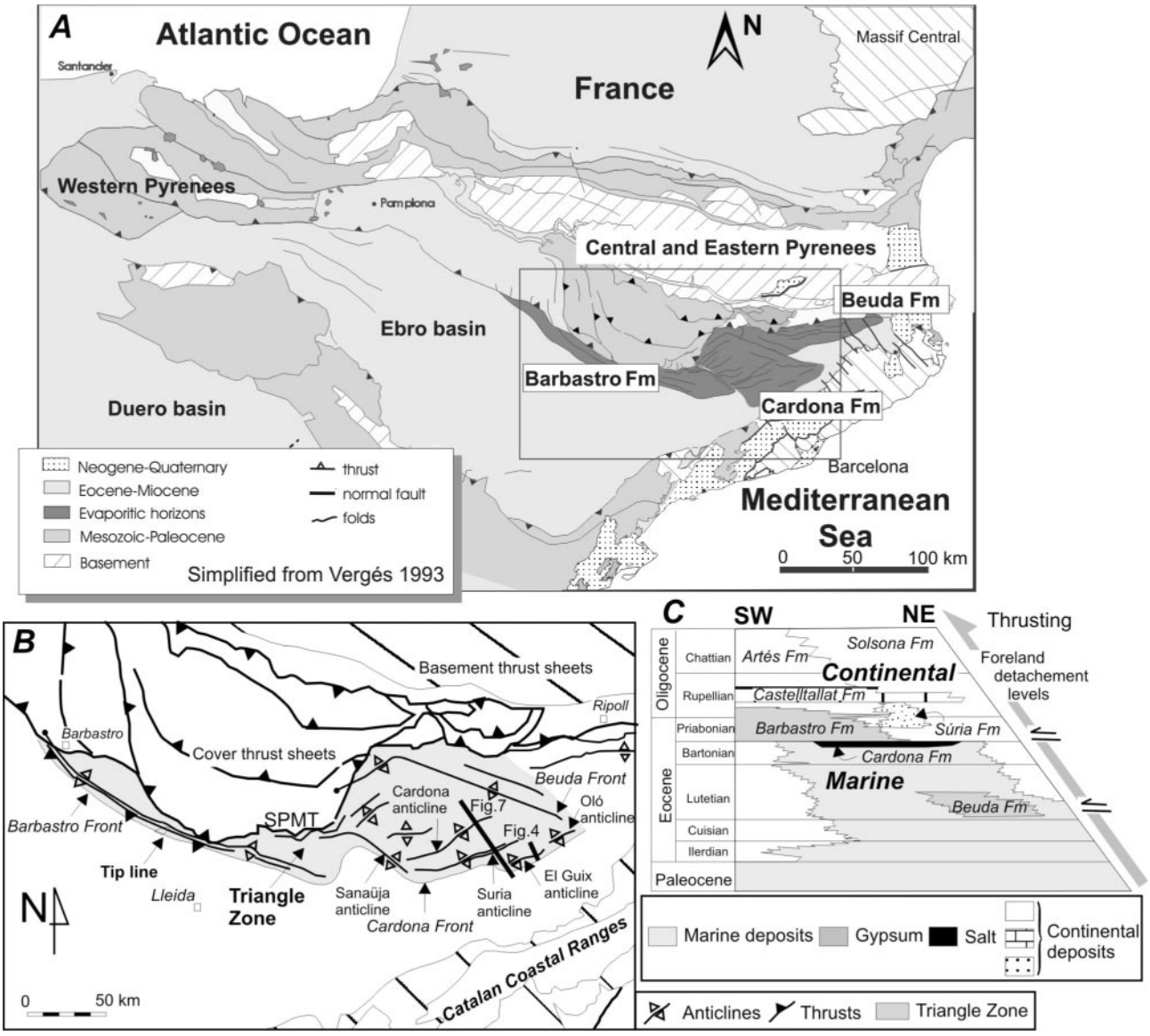


FIGURE 1 **A) Structural map of the Pyrenees (modified from Vergés, 1993). The area detached above the Beuda, Cardona, and Barbastro Fms. is shaded in dark gray. The Cardona Fm. extends westwards under the thrust sheets. The Barbastro Fm. partially overlaps with the Cardona Fm. Square shows the location of Fig. 1B. B) Structural sketch of the South Pyrenean Triangle zone (in gray). The three evaporitic levels are the stair-case basal detachment of the triangle zone. Three thrust fronts with different characteristics develop where the detachment level changes and are represented at the surface by a fold. Above each detachment, folds and thrusts of different orientations develop. SPMT stands for South Pyrenean Main Thrust. C) The sedimentary pile of the studied area is summarized in this schema and the location of the three main detachments is shown.**

which permitted recognition of the internal structure; good quality seismic profiles of the area were available; the southern Pyrenees are also characterized by good field exposures of the overburden and geologists have good knowledge of the structure, sedimentology and timing of deformation (Pueyo, 1975; Riba et al., 1983; Busquets et al., 1985; Agustí et al., 1987; Sáez, 1987; Anadón et al., 1989; Muñoz, 1992; Vergés et al., 1992; Vergés, 1993; Ayora et al., 1995; Vergés et al., 1995; Meigs et al., 1996; Rosell and Pueyo, 1997; Gil and Jurado, 1998; Vergés et al., 1998).

The basis of this study is the combination of field work with the subsurface data available and the elaboration of several analogue models (Fig. 2). The field work consisted of mapping selected areas at 1:10.000 scale along and across the South Pyrenean Triangle zone, especially on the El Guix, Súria and Sanaüja anticlines of the Cardona thrust front (Fig. 1). The field work in the overburden was complemented with the sampling for the analysis of the internal deformation and more detailed work in selected areas of the anticlines. The cross-sections have been constructed from the combination of field and subsurface data. The subsurface data consisted of over 50 potash exploration wells, and over 200 km of good quality seismic lines. The seismic lines which image the Súria and Sanaüja anticlines were shot in 1990, are confidential and belong to Súria K, S. A. and ENRESA. Finally, field work was also carried out in the Cardona diapir and underground mines which, together with the analysis of the data from exploitation areas of the mining companies Súria K, S. A., Potasas del Llobregat, permitted a good understanding of the internal structure of the detachment horizon. Together with this traditional approach, analogue modeling was carried out at the Hans Ramberg Tectonic Laboratory of Uppsala to test the influence of several parameters on the evolution of the salt cored structures, and the behavior of multiple detachment horizons.

## GEOLOGICAL SETTING - THE SOUTH PYRENEAN TRIANGLE ZONE

The southern Pyrenees consist of basement and cover thrust sheets which were displaced southwards from Late Cretaceous to Early Miocene as a result of the continental collision between the Iberian and European plates (Muñoz et al., 1986). The geometry of the South Pyrenean front varies from east to west. In the western part, west of Barbastro (Fig. 1A), the South Pyrenean Main Thrust emerges to the surface and superimposes Mesozoic rocks on an autochthonous undeformed foreland. In the central and eastern Pyrenees, the Ebro foreland basin is deformed by fault-related folds and thrusts defining a buried thrust-front. The tilted beds in the southern limbs of the frontal anticlines have been in most cases transported passively towards the hinterland along a passive roof thrust. As a result, the thrust-front has an intercutaneous wedge geometry (Sans et al., 1996a). The tip-line can be located in this area up to 40 km south of the South Pyrenean Main Thrust (Vergés et al., 1992).

This intercutaneous thrust wedge is the frontal wedge of the South Pyrenean Triangle zone. The term triangle zone is used in the sense of Gordy et al. (1977) as the strata between the basal blind thrust, the hinterland-verging thrust and the most external of the foreland-verging thrust to intersect the surface disregarding its internal structure. Defined in this way (Sans et al., 1996a), the South Pyrenean Triangle zone narrows to the west and ends where the most external structure is located in the footwall of the South Pyrenean Main Thrust (Fig. 1B). Eastwards, the triangle zone disappears by progressive attenuation of the frontal thrust wedge. The frontal structure of the easternmost Pyrenees, south of Ripoll (Fig. 1), is a detachment anticline on top of the buried tip line of the basal Pyrenean detachment (Fontboté et al., 1986; Muñoz et al., 1986). The irregularity in the geometry of the triangle zone as it is traced along-strike results from variation in the geometry of the South Pyrenean Main Thrust and in the trend of the frontal thrust wedge. The former is inherited from the geometry of the Mesozoic extensional basins and the latter is controlled by the southern pinch-outs of the three foreland evaporitic horizons (Vergés et al., 1992; Sans and Vergés, 1995). Moreover, the South Pyrenean Triangle zone has two of the most important requisites for triangle zone formation and preservation: presence of ductile detachments (Sans et al., 1996a; Cousenz and Wiltchsko, 1996) and moderate displacement (Hatcher, 1999).

The stratigraphy of the eastern Pyrenean foreland basin involved in the triangle zone is summarized in Fig. 1. The sedimentation changed from marine to continental during the emplacement of the thrust sheets (Puigdefàbregas et al., 1986). The marine infill of the basin ended after deposition of the Cardona salt in early Priabonian times. The Cardona Fm. consists from bottom to top, of anhydrite (5 m), a lower salt member represented by massive halite (200 m), and an upper evaporitic member of halite and interbedded potassium salt (50 m) (Pueyo, 1975). The transition of these marine sediments to the continental ones above takes place in a 60 m thick lutitic unit with interbedded gypsum and halite (gray lutites of Sáez, 1987). Continental deposits above the Cardona salt are represented by alluvial, fluvial and lacustrine sediments. The lacustrine deposits are represented in the study area by the Barbastro and Castelltallat Fms. of Late Eocene-Oligocene age (Sáez and Riba, 1986; Sáez, 1987; Anadón et al., 1989). The Barbastro Fm. consists of 30 m of gypsum and interbedded lutites and the Castelltallat Fm. is represented by 100-200 m of marls and interbedded limestones. These lacustrine deposits are interbedded with and

pass laterally, southward and northward, into the alluvial and fluvial sediments (Súria, Solsona and Artés Fms.). The Solsona and Artés Fms. are fine-to-coarse grained red sediments interpreted as alluvial fan deposits. The Artés Fm. has its origin in the Catalan Coastal Ranges. The Solsona Fm. was shed from the Pyrenees and grades to the south to the Súria Fm. sandstones, which have been interpreted as terminal alluvial fan deposits (Sáez, 1987). The uppermost deposits in the eastern Ebro foreland basin can be assigned to the upper part of the Lower Oligocene.

The tectonic style of the triangle zone's internal structure is characteristic of folded strata overlying evaporites (Davis and Engelder, 1985; Harrison and Bally, 1988; Harrison, 1991). The synclines are wide and flat bottomed and separate narrow and complex anticlines. The anticlines are salt cored, have no dominant vergence, have been cut by north and/or south-directed thrusts and some, as in the case of the Cardona anticline, have been overprinted by diapirism. The orientation of these folds allows the triangle zone to be divided in three areas. A northeastern region with ESE-WNW trending structures, a central region with NE-SW trending structures and a southwestern region with ESE-WNW trending folds and thrusts (Figs. 1A and B). Each of these three areas is located above a different evaporitic formation of the foreland. The

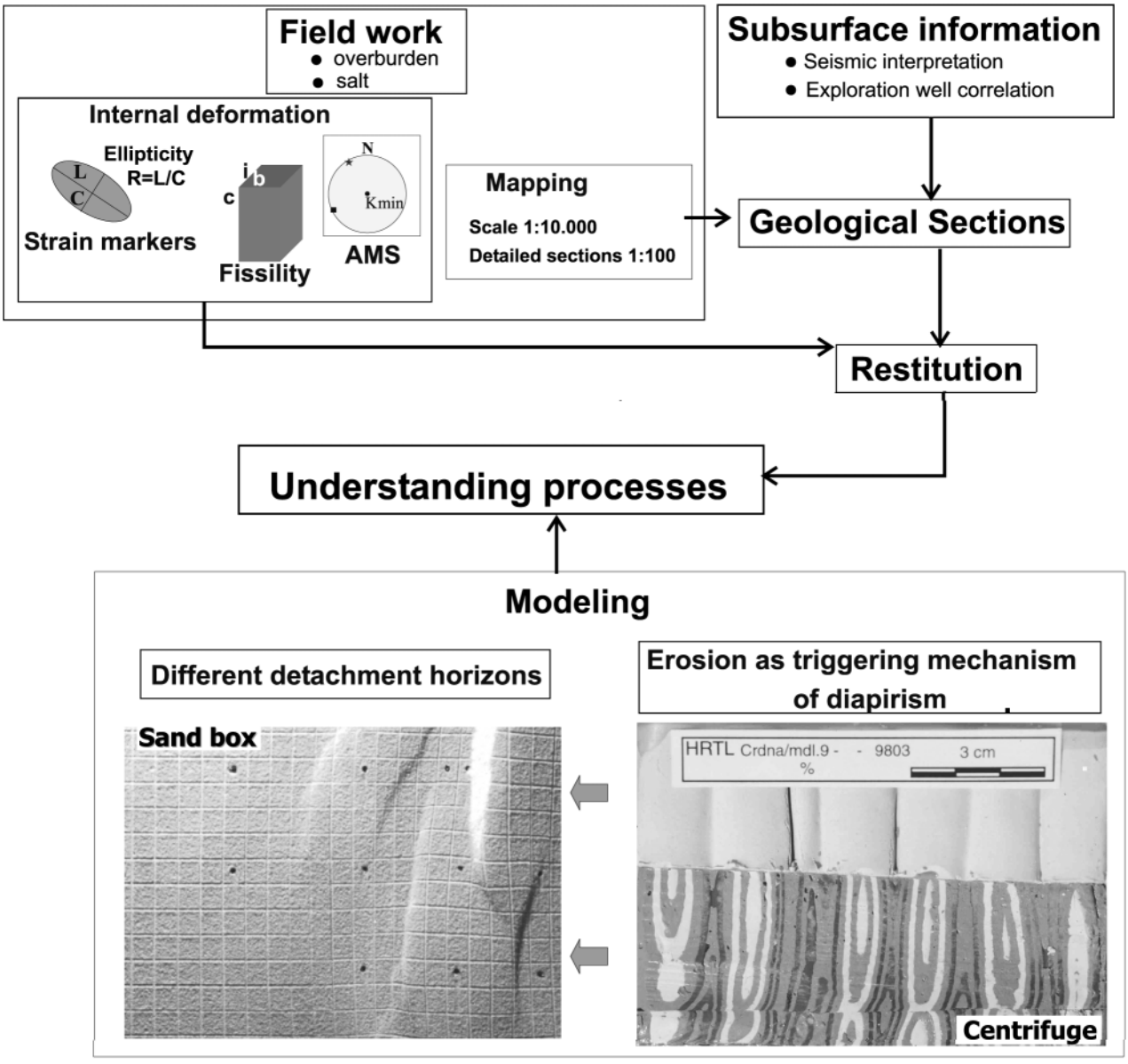


FIGURE 2 **This figure shows the methodology used in this work, which integrates field work with subsurface data as well as with analogue modeling and the study of internal deformation.**

northeastern region is located above the Beuda Fm., the central region above the Cardona Fm. and the southwestern region above the Barbastro Fm. These three horizons constitute the triangle zone's basal detachment which has a staircase geometry. Wide flats develop in the evaporitic Fms., ramps form coinciding with their southwestern edges and buried tip lines are present in their southeastern ones. This difference between the southwestern and southeastern margins is related to the oblique arrangement of the evaporitic basins with respect to the thrust transport direction (Vergés et al., 1992; Sans and Vergés, 1995).

The changes in orientation of the fold and thrusts at the surface correspond at depth with thrust wedges developed along the southern margins of the evaporitic basins (Figs. 1A and 1B). The northern thrust wedge is located at the southern pinch-out of the Beuda Fm. where the basal thrust climbs up into the Cardona salt Fm. The Oliana and Puig-reiganticlines represent the surface structure of this ramp (Vergés, 1993; Sans et al., 1996a). The intermediate wedge coincides at the surface with the Santa Maria d'Oló, El Guix, Súria and Sanaüja anticlines and it is related to the southern pinch-out of the Cardona salt. The southernmost wedge which lies on top of a buried tip line located at the edge of the Barbastro Fm., is represented at the surface by the Barbastro-Balaguer anticline.

## ROLE OF EVAPORITIC DETACHMENTS IN THE FORMATION OF TRIANGLE ZONES

Triangle zones have been the subject of great interest for geologists because they contain significant hydrocarbon reserves through-out the world, and because by "through studying triangle zones we can catch a glimpse of the processes that are at work throughout the formation of the orogenic belt, a snapshot of the deformation front that has not been obscured by subsequent deformation or obliterated by erosion" (MacKay et al., 1996). Although the best known triangle zone in the world is probably that of the Canadian Rocky Mountains, where the terminology of triangle zone and tectonic wedge were defined (Gordy et al., 1977), many other fold-and-thrust belts have developed this geometry at their front. Cousenz and Witchsko (1996) compiled 31 examples of different ages in thrust-belts throughout the world. Most of them have in common that they developed above ductile detachments composed either by shales, salts or other evaporites, and that they are located in frontal positions in the thrust belt.

The study of the South Pyrenean Triangle zone and of the models with multiple detachment levels (Sans, 1999) indicates that the geometry of the thrust-front in the fold-and-thrust belt is greatly influenced by the mechanical stratigraphy involved. In the southern Pyrenees the presence of evaporitic detachments coincides with a triangle zone geometry in the thrust-front. In contrast, where the evaporitic horizons are absent, the frontal thrust cuts through the syntectonic sediments or soles a foreland-vergent detachment-fold. Moreover, in the triangle zone, although the three fronts have evolved similarly, they have different geometries related to the mechanical behavior of the involved strata (Sans et al., 1996a). The Beuda and Barbastro thrust-fronts have as a main detachment level sediments consisting of shales, gypsum and some salt, whereas the Cardona thrust-front has as a main detachment level a thick salt horizon. Where salt is involved in the frontal thrust wedge it flows to form a salt cored anticline (Santa Maria d'Oló and Súria anticlines). Where gypsum or/and shales-marls are involved in the thrust wedge an antiformal stack develops (Oliana and Barbastro-Balaguer anticlines).

Similar results are shown in the two analogue models prepared in this work (Fig. 3) to simulate the presence of multiple detachments in a frontal area of a thrust belt. Each model consists of three ductile layers interbedded with layers of loose sand. The rheology of each layer was similar in both experiments as were the thickness and geometrical arrangement. The major difference in the two experiments is the amount of shortening undergone: model 6 was shortened to 15% and model 7 to 22%. Both values are in the range of shortening values achieved in the frontal part of the South Pyrenean Triangle zone.

The materials used in the models were clean Polydimethylsiloxane (PDMS) for the ductile layers and quartz sand for the overburden. The layers of pure PDMS have a viscosity of $5x10^4$ Pa s (density 0.987 g $cm^{-3}$). The layers of impure PDMS are one order of magnitude more viscous, e.g. $5x10^5$ Pa s (density 1.1 g $cm^{-3}$).The dimensions of model 6 were 30 x 47 cm. It was shortened from one end perpendicular to the width (Fig. 3). It consisted of three layers of Polydimethylsiloxane (PDMS), smaller than the model and arranged in a lateral and frontal stepping-up order. The bottom PDMS layer (lower ductile layer) was of impure silicone, 0.5 cm thick, and it covered an area of 15 x 15 cm. This layer was located in the left corner of the model, attached to the rear wall representing a backstop. This layer was surrounded by sand and covered by a 0.8 cm layer of sand. A color marker separated the lower ductile layer and the sand layer. On top of this sand layer, and separated by another color marker, there was a layer of pure PDMS (intermediate ductile layer). This layer was 0.4 cm thick, 20 cm long and 14 cm wide and placed at 15 cm from the shortening wall and 8 cm from the right wall. This layer was surrounded by sand and covered partially by a color marker. On top of it, an impure 1 cm thick PDMS layer (upper ductile layer) was placed. This layer was 26.5 cm long and 11.5 cm wide and it was located at 3.4 cm from the right wall and at about 14 cm from the frontal wall. Finally the model was covered by 1.5 cm of sand with color markers at

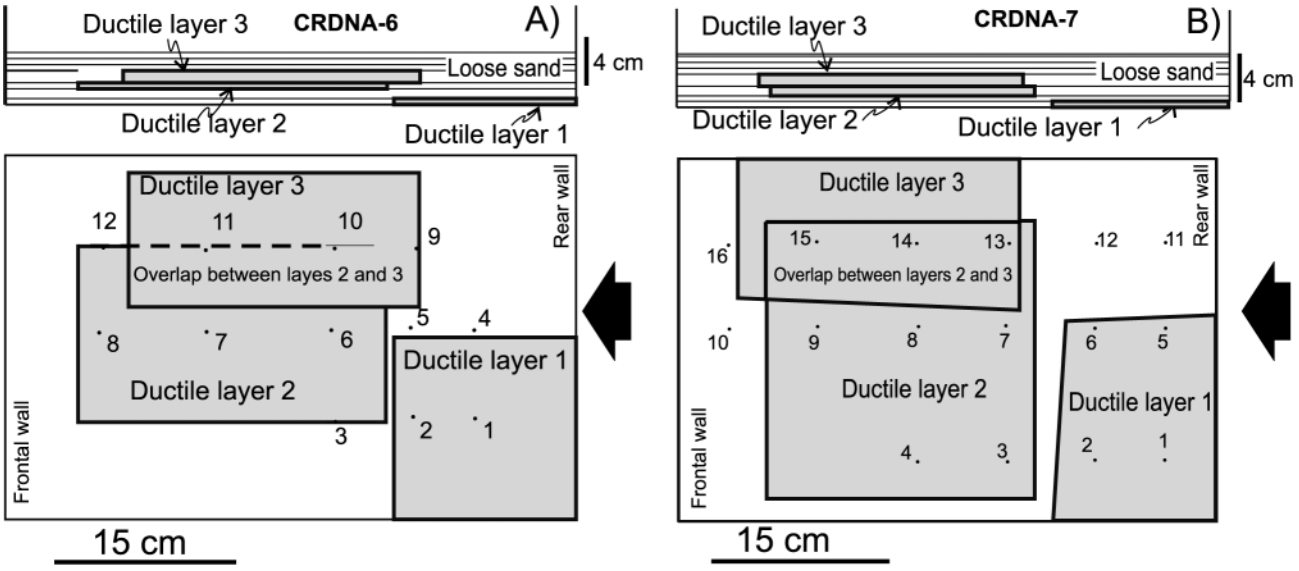


FIGURE 3 **Schema of the set up of the two models (CRDNA-6 and CRDNA-7) prepared with three detachment levels of different rheological properties which simulate the arrangement of the detachment horizons in the South Pyrenean Triangle zone. At the top there is a lateral view with the location and thickness of the ductile layers (in gray). At the bottom the location of the detachment levels from a top view, and the position of the measurement points. Arrow shows the sense of shortening. See text for detailed description. A) Model 6. B) Model 7.**

different heights (Fig. 3). The top of the models was gridded with a 1.2 cm by 1.2 cm square net and from the start, twelve points were printed in three longitudinal rows to monitor the horizontal displacement and vertical growth of the structures. The shortening velocity was 2 cm $hr^{-1}$ and the total shortening attained was 15%.

The dimensions of model 7 were also 30 x 47 cm and it was shortened as in model 6 from one end perpendicular to the width (Fig. 3). Model 7 consisted of three layers of PDMS, smaller than the model and arranged in a lateral and frontal stepping-up order. The bottom PDMS layer (lower ductile layer) was of impure silicone, 0.5 cm thick and slightly trapezohedral in shape. It was 16 cm wide and 15 cm long on the side of the model and 14 cm long in the center of the model. This layer was located in the left hand corner of the model, and attached to the rear wall, which represents a backstop. This layer was surrounded by sand and covered by 0.45 cm of sand. A color marker separated the lower ductile layer and the sand layer. On top of this sand layer, and separated by a color marker, there was a layer of pure PDMS (intermediate ductile layer). This layer was 0.8 cm thick, 22 cm long and 23 cm wide and placed at 16.5 cm from the rear wall and 2.5 cm from the left wall. This layer was surrounded by sand and covered totally by a color marker. On top of it was the upper ductile layer attached to the right wall and at 7 cm from the frontal wall. It consists of an impure 1 cm thick PDMS layer 25 cm long, 11.5 cm wide at the front of the model and 12.5 cm wide at the back. Finally, the model was covered by 1.5 cm of sand with color markers at different heights (Fig. 3). The top of the model was gridded with a 1.2 cm by 1.2 cm square net and from the start, sixteen points were marked in three longitudinal rows to monitor the horizontal displacement and vertical growth of the structures. The shortening velocity was 2 cm $hr^{-1}$ and total shortening reached was 22%.

The results of the two models suggest different development of triangle zones above a salt detachment and above a gypsum detachment. Above the salt detachment (pure PDMS), folding was the dominant deformation mechanism and wedges formed continuously at the deformation front through the fold-belt evolution (Fig. 4). Instead, above the gypsum detachment (impure PDMS), thrusting was the dominant mechanism and wedges only formed at the sedimentary pinch out of the evaporitic layer (Fig. 5). The rheology of the detachment horizons controls, thus, the geometry of the deformation front. Very ductile detachments (Cardona Fm. and pure PDMS) promote folding and triangle zones are formed at the deformation front along the deformation history. Where the detachment is less ductile (Barbastro and Beuda Fms., and impure PDMS), thrusting is the dominant deformation mechanism and the triangle zone geometry is formed only at the detachment pinch-out.

The syntectonic sediments related to the three thrust wedges in the South Pyrenean Triangle zone allow the wedges to be dated. Most of the syntectonic deposits are continental and their ages have recently been determined precisely by an extensive magnetostratigraphic survey (Burbank et al., 1992a, 1992b). Structures at the southern

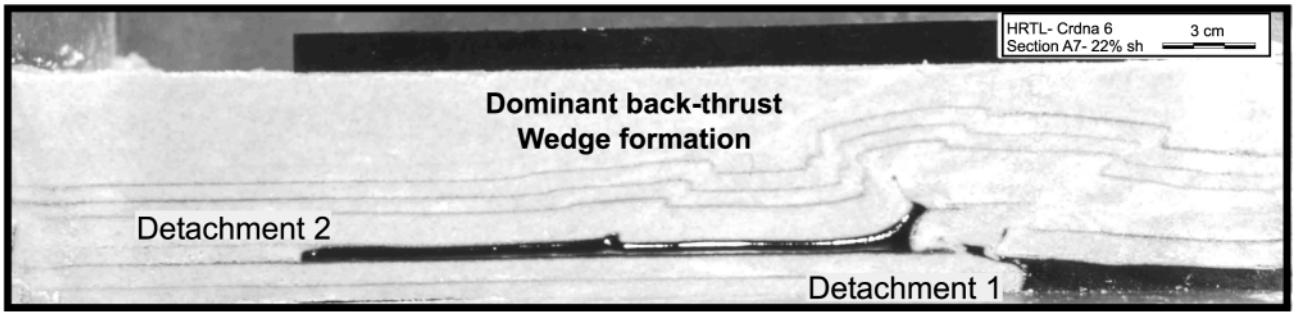


FIGURE 4 **Section of model CRDNA-6. Above detachment 2 (pure PDMS) there is a dominance of backthrust even if the structure being formed is not located at the tip point of the detachment. Compare with Fig. 5.**

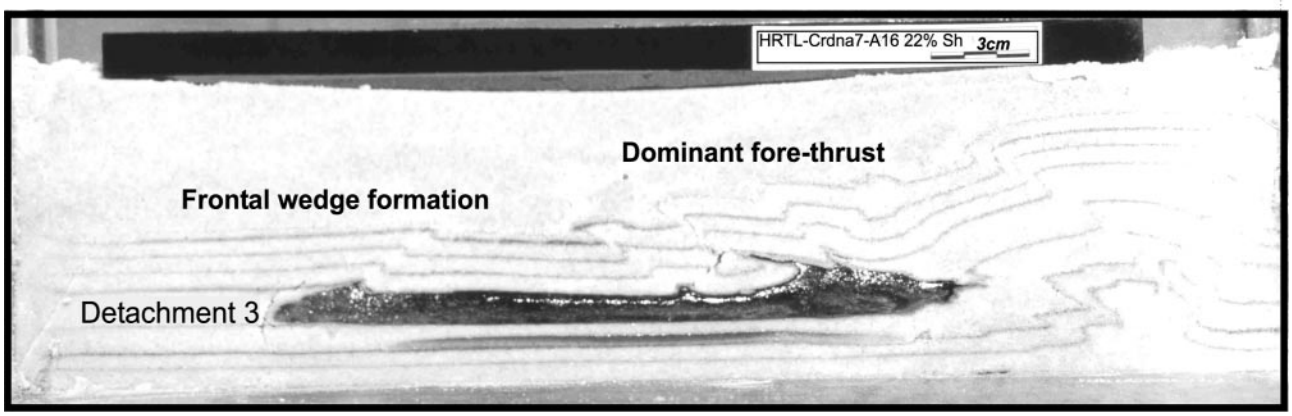


FIGURE 5 **Section of model CRDNA-7. Above detachment 3 (impure PDMS) there is a dominance of fore-thrust and only at the tip point of the detachment a backthrust, and therefore a wedge is formed. Compare with Fig. 4.**

limit of the Beuda Fm. (Puig-reig and Oliana anticlines) developed after deposition of the Cardona salt during Late Eocene-Early Oligocene times (Burbank et al, 1992a). Structures at the limit of the Cardona Fm. (Santa Maria d'Oló, Súria and Sanaüja anticlines) deformed uppermost Lower Oligocene deposits (Sáez, 1987). Structures in the western extremity of the Sanaüja anticline involve fluvial and lacustrine sediments interpreted as Lower and Upper Oligocene by magnetostratigraphy (Meigs et al, 1996). Farther south and west, the Barbastro-Balaguer anticline has been dated as Late Oligocene-Early Miocene (Pardo and Villena, 1979; Riba et al., 1983; Senz and Zamorano, 1992). From these ages the three wedges are considered to have been the successive frontal structures of the triangle zone during its development. The preservation of several subsequent triangle zones in the South Pyrenean foreland has been possible because the total tectonic displacement towards the foreland was small. The field evidences suggest that triangle zones form when the basal decollement meets a ductile detachment and that they are not necessarily the last stage of deformation in a fold-and-thrust belt history. This is also shown by the results of the monitoring points in the analogue modeling which show that the frontal wedges were active during a certain period of time and were abandoned once the sole thrust climbed to a stratigraphically higher detachment level and propagated towards the foreland (Sans, 1999).

The lateral evolution of the triangle zone in the South Pyrenean foreland shows that with the increased shortening along strike, the frontal wedge evolved from detachment folds, through antiformal stacks to passive-roof duplexes. Each of the described fronts (Beuda, Cardona and Barbastro) evolved from east to west from a detachment fold, through an antiformal stack to a passive roof duplex involving a progressive increase in the amount of shortening in the same direction (Sans et al., 1996a). The frontal thrust wedge deformation migrated to the SW in agreement with the overall decreasing age for the end of the Pyrenean orogenesis from east to west (Vergés, 1993). The lateral continuity of the typical triangle zone frontal geometries with the salt-cored detachment folds with hinterland-vergence suggests that these detachment folds could be considered as an incipient stage of the frontal thrust wedge in the triangle zone development (Sans and Vergés, 1995). The frontal wedge of this part of the triangle zone could be

considered a ductile wedge where deformation was distributed in the ductile layer coring the anticline.

Reactivation of previous foreland-directed thrusts as hinterland-directed during triangle zone formation is suggested in the South Pyrenean Triangle zone in the western part of the Cardona thrust-front (Sanaüja anticline). In this area, salt and gypsum layers are involved in the frontal-thrust wedge (Fig. 6). The frontal backthrust is located in the upper part of the gypsum levels separating undeformed gypsum beds above it from deformed gypsum beds below it. The internal structure of the salt and gypsum levels shows disharmonic foreland-vergent folds, even in the southwestern limb of the Sanaüja anticline (Sans et al., 1996a, 1996b). These folds have been related with a generalized top-to-the-foreland shear previous to folding and thrusting. Therefore the present day frontal backthrust in the southwestern limb of the Sanaüja anticline was a foreland-directed detachment during the first stages of deformation. At an outcrop scale, small thrusts in the detrital series overlying the salt and gypsum levels are cut by backthrusts. Field relations show, thus, that foreland-verging structures are older than hinterland-directed ones in the Sanaüja anticline. The same type of relationships between foreland-directed structures and hinterland-directed ones are observed in the Barbastro frontal thrust wedge (Sans et al., 1996a). As in the Sanaüja anticline, the hinterland-directed upper detachment of the thrust wedge only developed after a certain amount of growth of the frontal anticline. In both examples the hinterland-directed upper detachment reactivated previous foreland-directed detachment.

## STYLE OF FOLDING

The folds developed above the Cardona Fm. can be subdivided into three groups according to their geometry: in the first group, the Vilanova, l'Estany and Cardona anticlines; in the second group the Sanaüja anticline and in the third group, the Súria and El Guix anticlines. The first group is formed by anticlines developed where the Cardona Fm. is thickest (approx. 300 m) and where the basal slope of the Cardona Fm. is low (~0º). They are mainly detachment anticlines characterized by uplifts between 900 and 1200 m and wavelengths between 10 and 15 km. They are locally cut by thrusts, specially towards the west where the accumulated shortening is larger. The Cardona anticline is foreland-vergent whereas the Vilanova is symmetric. The syncline separating the anticlines is welded with the subsalt strata leaving each anticline as a closed system that will evolve independently. The second group is only represented by the Sanaüja anticline. This anticline formed in the western limit of the Cardona Fm., and represents the surface

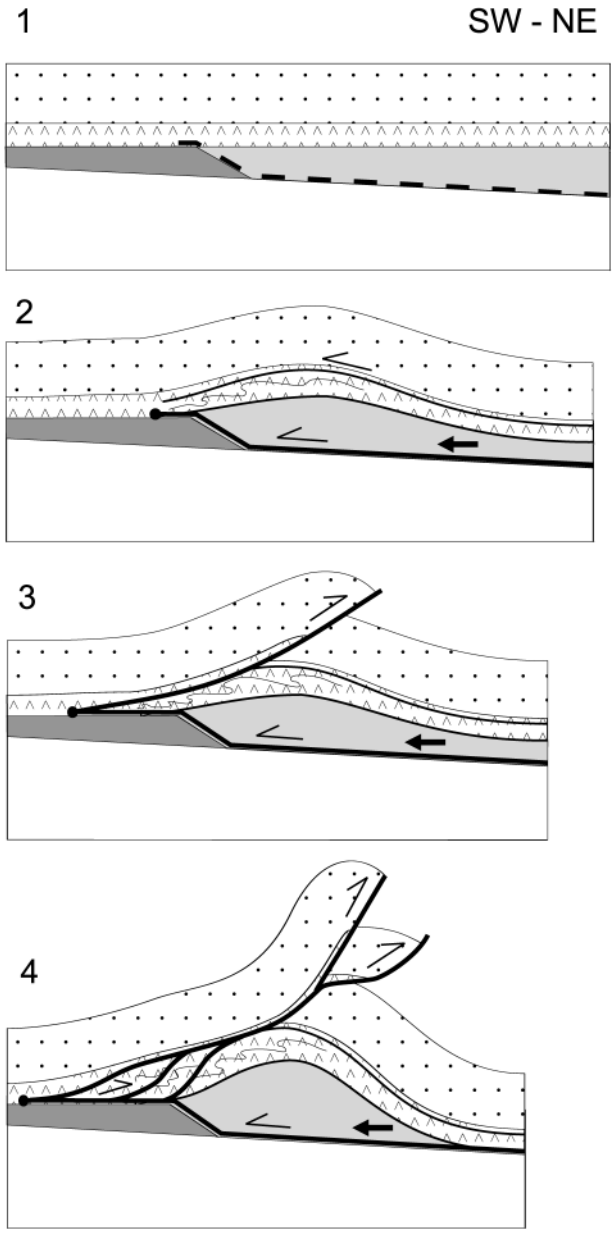


FIGURE 6 **Evolution of the Sanaüja anticline (from Sans et al., 1996a). 1) Initial geometry of the Cardona salt (gray), the Barbastro gypsum (inverted v symbols) and the clastic cover (dotted). 2) Salt migrated from the northeast into the anticline and folds developed in the Barbastro gypsum related tot he shear sense in the detachment. 3) A backthrust reactivated previous foreland-directed structures and separated folded gypsum layers from non-folded gypsum layers. 4) Salt flow from the northeastern limb continued at the same time that a hinterland-directed duplex developed in the Barbastro Fm.**

expression of the ramp between the Cardona and the Barbastro detachments (Vergés et al., 1992; Sans et al., 1996a). At surface, it outcrops as a symmetric anticline, but both limbs have a different structure. The northeastern limb is characterized by a withdrawal of the Cardona salt and relatively undeformed beds over it, whereas the

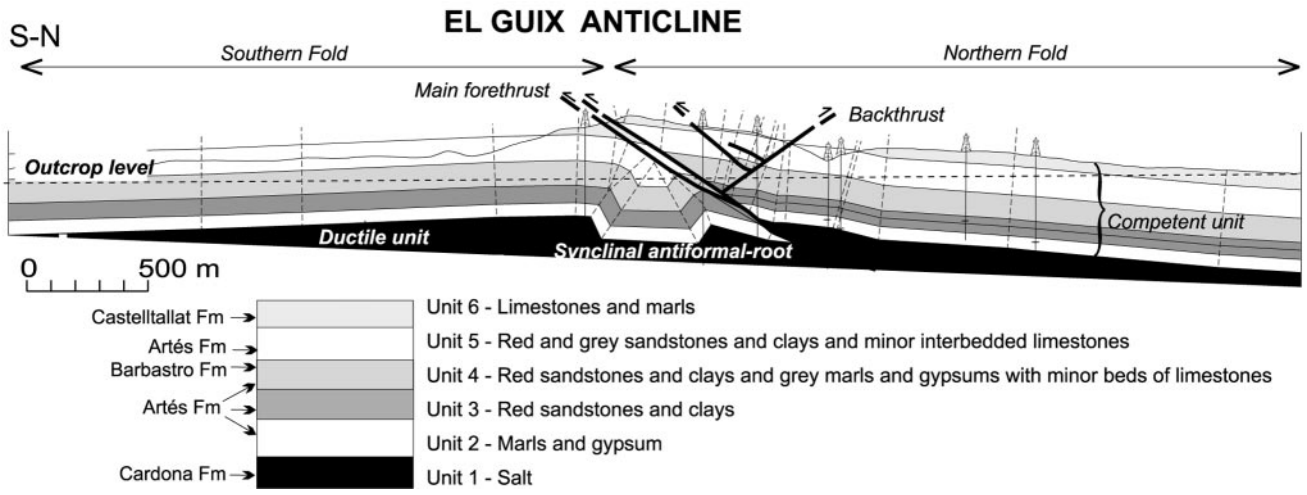


FIGURE 7 **Section of the El Guix anticline. At surface this anticline is a large wavelenght/amplitude ratio anticline cut by a south-directed thrust, and characterized by long limbs of relatively low dip (<4º). At depth the structure of the anticline is more complex and consists of two anticlines of opposite vergence facing each other separated by a syncline which is called the synclinal antiformal-root. These synclines can also be seen in other anticlines of the area such as the Súria anticline (see Fig. 11).**

southwestern limb is characterized by a hinterland-directed duplex in the Barbastro Fm. (Fig. 6). Finally, the third group of folds developed in the southern pinch-out of the Cardona salt. The structures developed in this area, like the El Guix and Suria anticlines show some intriguing features such as synclinal antiformal-roots, and double vergence.

Synclinal antiformal-roots are deep structures which form below the anticline crest. They consist of synclines that sink into the ductile layer and separate folds of facing vergence. They are especially well exposed in the El Guix anticline (Fig. 7) and imaged by the seismic lines in the Suria anticline (Sans and Vergés, 1995; Sans et al., 1996a).

To understand the influence of the shape of the detachment level and of the thickness ratio between the overburden and the ductile layer in the formation of synclinal-antiformal roots, six models were prepared (Fig. 8). The materials used were Polydimethylsiloxane (PDMS) to simulate the salt layer and quartz sand to simulate the overburden. Each of the models consisted of a basal ductile layer of impure PDMS ($5x10^5$ Pa s, density 1.1 g $cm^{-3}$) resting on a slope. The PDMS layer only covered a part of the base of the model, from the back of the model to a certain distance, depending on the basal slope. In each model the ductile layer was overlaid by different overburden thickness (Fig. 8). The models were shortened at 2 cm $h^{-1}$ by up to 12%, only model CRDNA-5 was shortened up to 14%. In the models, the surface was gridded (1.2 cm x 1.2 cm) and the lateral and vertical displacements were monitored by several points marked on the surface of the model (Fig. 8).

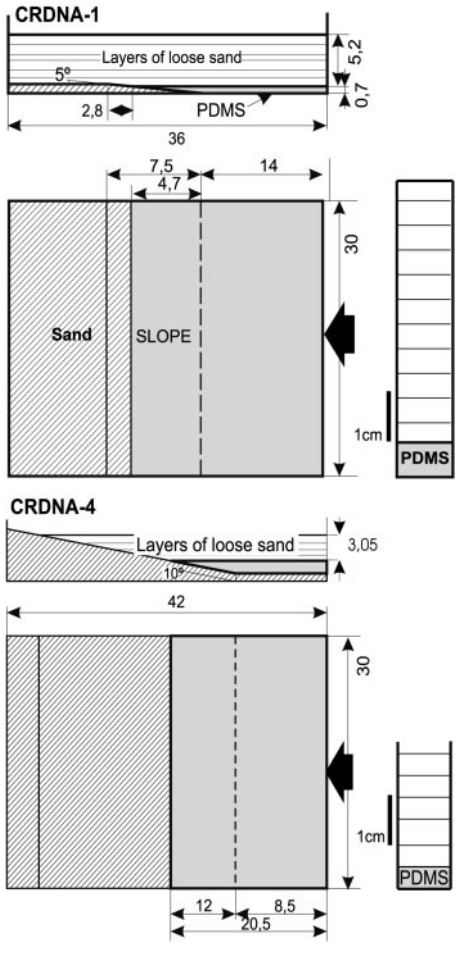


FIGURE 8 **Set up of two analogue models (CRDNA-1 and CRDNA-4) with different overburden/salt layer thickness and basal slopes. For each model the lateral view, the top view and the stratigraphic column are drawn. Arrow indicates de sense of shortening.**

In the models, the synclinal antiformal-roots formed in the first stages of deformation as a result of the intersection of the kink bands downwards (Fig. 9). The intersection of the kinks takes place within the overburden layers, above its boundary with the underlying ductile layer (Sans, 1999). These synclines are ephemeral and with increasing deformation they become more asymmetric, tighter and rotate to parallelism with the overlying beds. As a result, at 12% of deformation they are more difficult to identify than at 4% or 6% of deformation. They are not continuous along-strike and seem to be preferentially associated with symmetric rather than with asymmetric box folds (Fig. 10). The synclinal antiformal-roots formed in the models are very similar to those observed in the El Guix and Súria anticlines (Figs. 7 and 11). The botton layer of the synclinal roots are below the initial regional elevation of the top of the ductile layers and are located directly beneath the anticlines. The El Guix anticline (Fig. 7) can be easily compared to model 1 (Fig. 9) and the early stages of deformation of model 4. In both models a symmetric syncline formed under the anticline. In the Súria northern anticline, the syncline is not present along the strike of the structure (Sans and Vergés, 1995). It has only developed in the area in which the fold changes from a symmetric to an asymmetric anticline. Although the Súria northern anticline is not a box fold anticline and the presence of a secondary detachment higher in the section gives the anticline a wedge structure (Fig. 11), the synclinal antiformal-root is similar to those developed in models 1, 2 and especially in model 4 (Fig. 10).

In the models, the synclinal antiformal-root becomes asymmetric with increasing deformation. In symmetric synclinal antiformal-roots the two intersection points between the fore and back kink lie in the same vertical (Fig. 12A). In models 1 and 4 the two intersection points were not in the same vertical and the synclinal antiformal-root was asymmetric (Fig. 9). Asymmetric synclinal antiformal-roots in-dicate a dominance of one of the kink bands (Fig. 12). In model 1 the intersection point in the synclinal antiformal-root was slightly behind the intersection point in the anticline suggesting a further slip of the front kink (Fig. 9). In contrast, in model 4 the intersection point on the synclinal root was slightly in front of the intersection point in the anticline suggesting a further slip of the back-kink (Fig. 10). The El Guix anticline is cored by a back-directed synclinal antiformal-root which gives a higher uplift to the southern anticline than to the northern one. The double anticline is cut later on by a fore-thrust (Fig. 7). In this case, the anticline is eroded and the backthrust mapped in the field is not the equivalent to the back-kink of the model, since this would have been displaced upward by the frontal thrust and eroded.

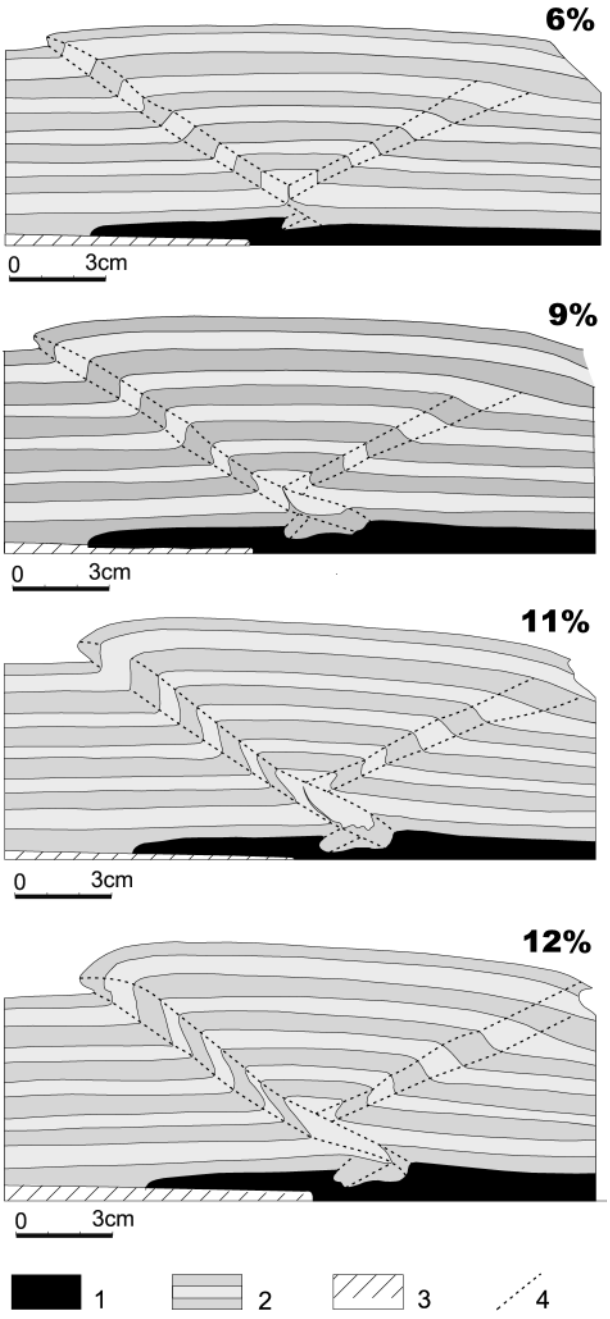


FIGURE 9 | **Schema of the evolution of model CRDNA-1. A synclinal antiformal-root develops at the first stages of deformation (before 6%). With increasing shortening the root becomes wider and separates two facing anticlines at depth, whereas the surface structure corresponds to a unique anticline. The fore-kink dominates and the back-kink is displaced upwards with increasing deformation. At the final stage (shortening 12%) the synclinal antiformal root is well developed in the model. 1: PDMS (salt); 2: alternating sand layers (overburden); 3: bottom slope.**

The results from the models and field examples show that synclinal antiformal-roots located in the cores of anticlines form only above ductile detachments which allow them to sink into them. However, this is not the

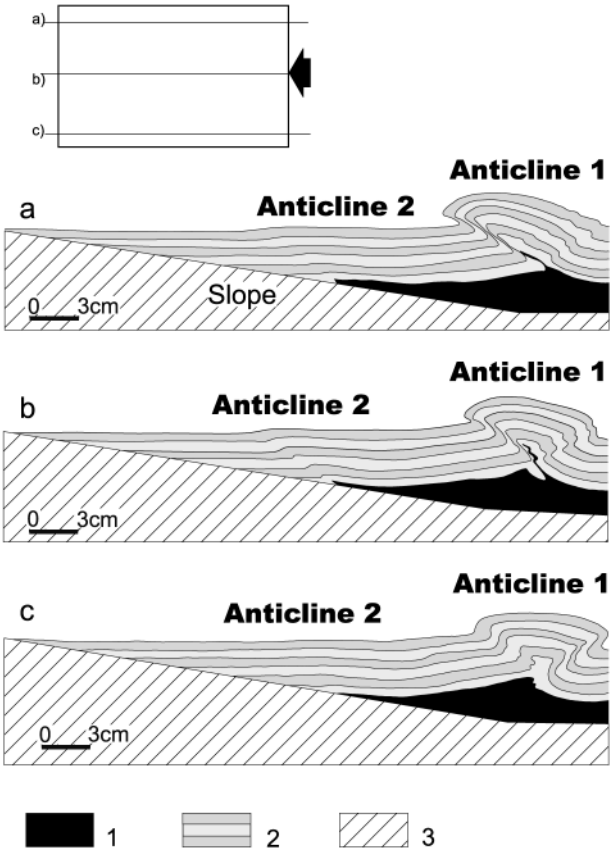


FIGURE 10 **Three longitudinal and parallel sections of model CRDNA-4 at 12% shortening. Inset shows a sketch of the location of the sections in a top view of the model and arrow indicates the sense of shortening. In all sections two folds are present across the model. The frontal fold developed at the pinch out of the PDMS layer. Under the larger fold, in the back of the model, a synclinal antiformal-root can be observed where the anticline is symmetric, and specially in the transition zone from a symmetric to an asymmetric anticline (sections b and c). This feature cannot be observed where the anticline is fore-vergent. 1: PDMS (salt); 2: alternating sand layers (overburden); 3: bottom slope.**

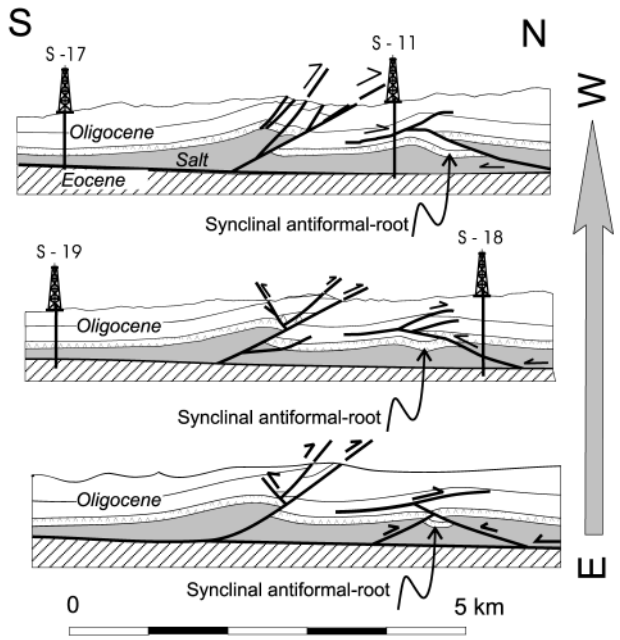


FIGURE 11 **In the Súria anticline, the deep structure of the northern anticline shows also the presence of a synclinal antiformal-root.**

only requirement. In model 3, which had a thin overburden and a low basal slope, synclinal roots were not formed. Model 3 was the only one in which three structures had formed after 12% shortening. This suggests that rapid fold growth and a small overburden/ductile layer ratio may inhibit the formation of a synclinal root. In the Cardona thrust-front, synclinal roots have not been identified under the anticlines located in more internal parts, where the initial salt thickness was higher and the slope was less. Although this subject needs further research, it suggests that easy slip above the basal detachment may also inhibit the formation of synclinal roots. In contrast, an increase in basal friction due to reduction of the salt thickness or an increase in basal slope may favor their formation.

## RELATIONSHIP BETWEEN THE STRUCTURE OF THE DETACHMENT AND THE INTERNAL DISTORTION OF THE OVERBURDEN. INSIGHTS INTO THE CHRONOLOGY OF DEFORMATION

In many fold and thrust belts, the overburden geometry and the external shape of the salt accumulations are known (Parry Islands, Morocco, Algeria, Jura, Sierra Madre Oriental), whereas very few studies document the internal structure of detachment horizons in evaporites (Marcoux et al., 1987; Jordan and Nuesch, 1989; Malavielle and Ritz, 1989). The internal structure of salt horizons has often been described as chaotic (Richter-Bernburg, 1980), and salt has been described as having short strain memory and only recording the last increments of deformation (Talbot and Jackson, 1987). The South Pyrenean Triangle zone offers a unique example to study the internal structure of a detachment since the Cardona salt horizon can be studied almost continuously for over 30 km in different salt mines (Fig. 13), from the deformation front to more internal positions (Sans et al., 1996b). Moreover, the salt has several distinct units which can be mapped and followed as guide levels for the metric to kilometric structures. For smaller size structures, the salt is thinly bedded and the clay levels are good external markers to record the deformation history of the detachment. Also, the fact that the amount of shortening in the study area is moderate and the displacement small permits the development and preservation of simple structures in the detachment horizon.

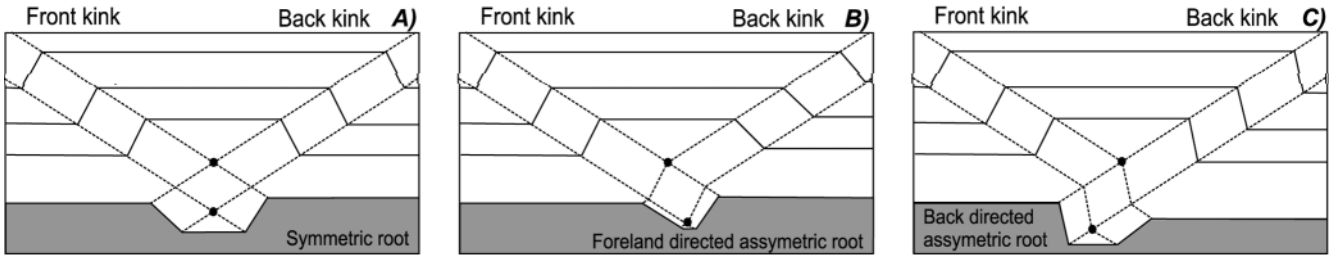


FIGURE 12 | **A) Symmetric synclinal antiformal-root. B) Fore-directed asymmetric synclinal antiformal-root. C) Back-directed asymmetric synclinal antiformal-root.**

The study of the internal structure of the salt cored anticlines in the South Pyrenean Triangle zone has shown that it is neither chaotic nor random, but that it records the deformation history of the detachment and associated folds and thrusts (Sans et al., 1996b; Sans, 1999). Three events can be distinguished in the deformation history of the salt horizon, which are part of the same shortening episode (Sans et al., 1996b) (Fig. 14). First, a generalized shear motion with top-to-the-foreland was recorded by meter to tens of meters scale south-vergent folds and shear zones. This deformation is widespread in the salt horizon in all the structural positions studied. Second, large scale (kilometric) folding produced thickening of the salt toward the anticlines and thinning in the synclines as well as rotation of the folds formed during the generalized shear event (Sans et al., 1996a). Third, thrusting and back-thrusting were also recorded in the salt layer as south and north-vergent tight fold zones. This suggests that faults root through a ductile faulting zone with a detachment surface located deeper than the interface between the salt and the overburden. In the salt layer, as we approach a "fault zone", folds become tighter and the presence of minor shear bands at high angle to the bedding increases. The fault zones do not appear to be folded in the studied outcrops. There is also a spatial coincidence between the areas of possible maximum deformation with areas of barren bodies known as "estèrils"suggesting that during deformation there is migration of brines undersaturated in potassium through the shear zones. This may also be supported by the fabric analysis carried out in the halite levels (Miralles et al., 2001). Samples collected in the shear zones show a strong decrease of water content, and thin brine films at the grain boundaries, suggesting the operation of fluid assisted recrystallization processes during deformation.

These three events can also be seen in the overburden in the same sequence. Folding and thrusting are well observed in the field. However, the question arises as to which event was responsible for the generalized shear towards the foreland. Analysis of the strain markers provided evidence of a layer parallel shortening event previous to folding and thrusting which might provide an answer to this question.

## Sedimentary strain marker analysis

Good sedimentary strain markers are objects in which we can measure differences in shape before and after deformation. In this work, initially elliptical or circular objects

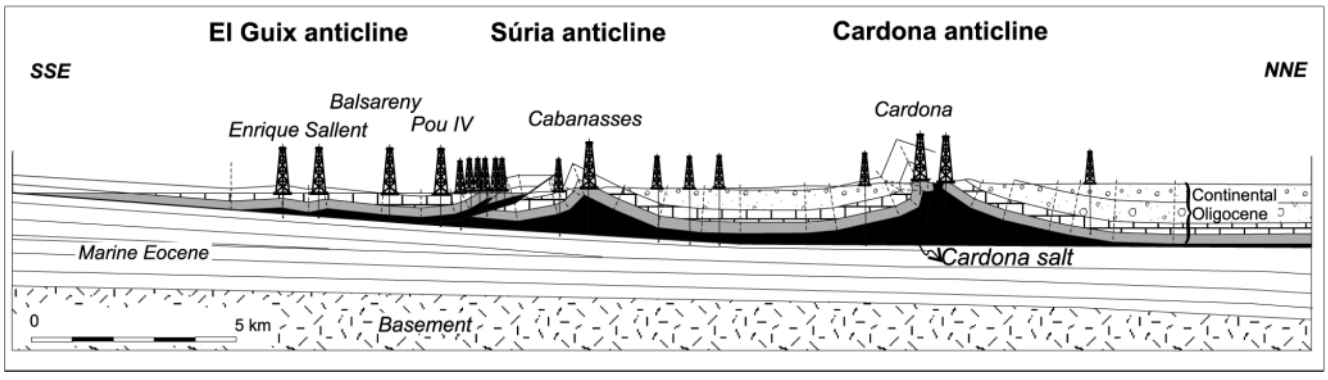


FIGURE 13 | **Section of the Cardona thrust-front across the El Guix, Súria and Cardona anticlines along the Cardener river. Each of these anticlines is mined for potash (larger well symbols). The information obtained from the different together with the information of many exploration wells gives an almost complete view of the structure of the detachment horizon from the deformation front to the most internal structures.**

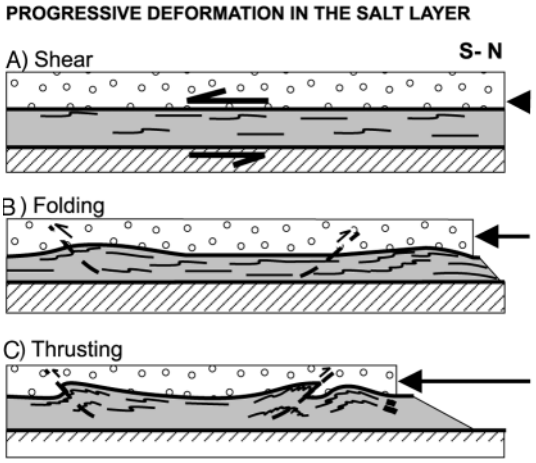


FIGURE 14 **Cartoon of the three main events in the deformation history of the salt layer (in gray) and the overburden (circles). A) Generalized shear with top-to-the-south motion. B) Large scale folding. The previous south-vergent folds can be seen in north limbs as well as back limbs. Only in very few locations they are rotated. C) Thrusting. In the salt horizon there is development of high angle shear zones and north and south-directed folds in relation with back or fore-directed thrusts.**

randomly oriented on the bedding plane, such as burrows, rain drops and oxidation marks were used. A total of 35 measurement stations (Table 1) along a regional section from the Cardona anticline to the El Guix anticline (Sans, 1999) were measured. The parameters analysed (Fig. 2) were the ellipticity Rf (ratio between the long and short axes of the ellipse) and the orientation Δ of the ellipse long axis. These two parameters were related in Rf/Δ data graphs to obtain the mean orientation and ellipticity of the analysed markers. All this procedure was done in a computer aided system. The long and short axis dimensions and Δ angle were measured by the IMAT program (Serveis Cientifico Tècnics de la Universitat de Barcelona, 1995). This program measures these parameters among others by a conventional image analysis of a scanned drawing of the oriented samples collected in the field. The Rf/Δ graph as well as the mean calculations were done by the program GRPRF developed by Durney (University of Macquarie, Australia, 1996). This program calculates the mean ellipticity of a set of ellipses by its iterative retrodeformation to an isotropic distribution (with a zero ln(Rf/2Δ) vector mean). Plane strain is assumed in order to correlate the measured ellipticities on the bedding plane with the strain ellipsoid (Sans, 1999). On this assumption and bearing in mind that cleavage is, where present, perpendicular to bedding, and that there are no evidences of along strike extension of the folds, the bedding plane contains the shortening direction and represents the YZ section.

The results of the markers analysis show that from the regional point of view, there is no significant differences in the layer parallel shortening values (LPS) between the

TABLE 1 **Ellipticity (Rf) and orientation (φ) values of the strain ellipse in the Cardona thrust-front.**

***Region: El Guix- Sallent***

| *Location* | *N of samples* | *Marker type* | *Rf* | *φ* | *N of measurements* |
|---|---|---|---|---|---|
| 1 | 1 | Burrows | 1,2 | 73 | 12 |
| 2 | 8 | Burrows<br>Oxidation marks<br>Rain drops | 1,2 | 71 | 186 |
| 3 | 3 | Burrows | 1,2 | 78 | 76 |
| 4 | 1 | Burrows | 1,2 | 72 | 14 |
| 5 | 2 | Burrows | 1,2 | | 104 |

***Region: El Guix- Callús***

| *Location* | *N of samples* | *Marker type* | *Rf* | *φ* | *N of measurements* |
|---|---|---|---|---|---|
| 6 | 1 | Burrows | 1,2 | | 27 |

***Region: Súria***

| *Location* | *N of samples* | *Marker type* | *Rf* | *φ* | *N of measurements* |
|---|---|---|---|---|---|
| 7 | 1 | Burrows | 1,3 | 47 | 10 |
| 8 | 2 | Burrows | 1,3 | 47 | 10 |

***Region: Cardona***

| *Location* | *N of samples* | *Marker type* | *Rf* | *φ* | *N of measurements* |
|---|---|---|---|---|---|
| 9 | 4 | Burrows | 1,2 | 62 | 102 |

***Region: Manresa***

| *Location* | *N of samples* | *Marker type* | *Rf* | *φ* | *N of measurements* |
|---|---|---|---|---|---|
| 10 | 3 | Burrows | 1,0 | | 56 |

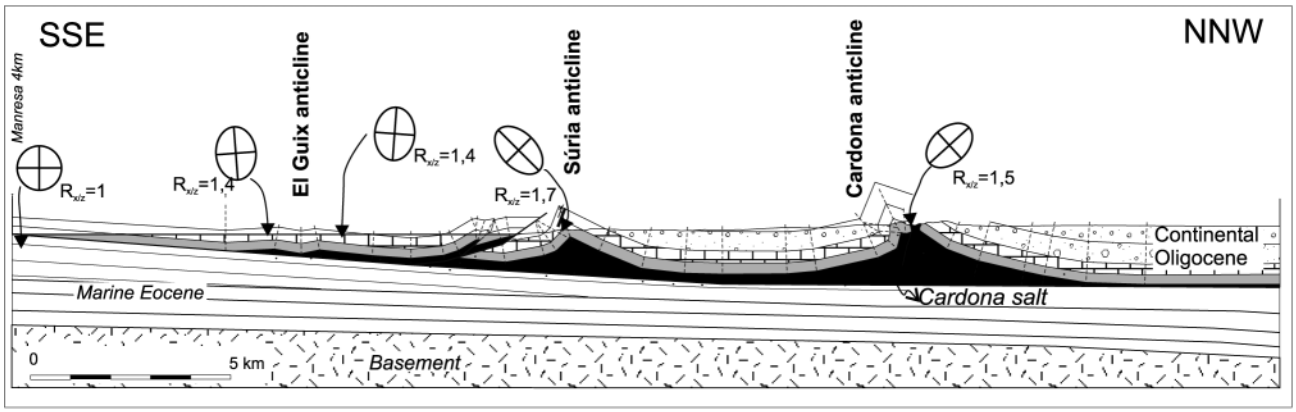


FIGURE 15 **Section of the Cardona thrust front along the Cardener river. Ellipses indicate the XZ section of the strain ellipsoid calculated from the markers on the bedding plane (YZ section) assuming plane strain (Y=1). Z is contained on the bedding plane. Squares show the relation between the c and b axis of the fissility fragments. Below the detachment, at the Manresa location (4 km to the south), the ratio between the X and Z axis is 1, which indicates that the rocks are not deformed.**

studied anticlines (Fig. 15; Table 1). In the plane of the section (parallel to tectonic transport) the values are $R_{x/z}$=1.2, (LPS=17% shortening) for the Cardona anticline, $Rf_{x/z}$ =1.3, (LPS=23% shortening) for the Súria anticline and $Rf_{x/z}$=1.2, (LPS=16% shortening) for the El Guix anticline. In contrast, there is a decrease in the $R_{x/z}$ value in the samples collected below the detachment, to the south, which can be considered undeformed ($Rf_{x/z}$=1.0). This corroborates the presence of a detachment at depth which permits a good decoupling of the cover. The little variation of the deformation values through a large area suggests that the detachment is a ductile detachment. The orientation (Δ) gathering is fairly good in the three anticlines and varies from N073E in the El Guix anticline to N060E in Súria and N047E in Cardona. In the three cases it is parallel to the local orientation of the large-scale structures where the internal deformation measurements were done (Fig. 1).

El Guix anticline was explored in more detail and 413 measures were carried out in its northern limb. The results show values of internal deformation ranging from $Rf_{x/z}$ =1.0 for incompetent burrows to $Rf_{x/z}$=1.2 in most of the measurements, giving a mean value of 1.2 (Fig. 15). This value ($Rf_{x/z}$=1.2) is also recorded in the same anticline, 8 km to the west suggesting, thus, no variation along the strike. It is important to emphasize that the orientation of the strain ellipses on the bedding plane calculated by the different sets of markers is the same after unfolding in samples collected in beds which are horizontal as in beds which are vertical. This reveals that the strain we are measuring preceded the verticalization of the beds. The parallelism between the markers long axis and the cleavage intersection on the bedding plane indicates that the deformation recorded by the markers corresponds to layer parallel shortening (LPS) achieved prior to folding and thrusting. Therefore the restoration of the overburden of the section of the frontal thrust wedge (El Guix double anticline) in the south central Pyrenees presented in this paper must take into account a bulk deformation split into 5% due to folding and thrusting and 16% due to the internal deformation by layer parallel shortening which is the main shortening mechanism in this area (Fig. 16).

The values of layer parallel shortening derived from the marker analysis are very constant in the studied anticlines and account for 16% to 23% of shortening. These values are two to three times larger than the shortening values calculated from the restitution of the macroscopic scale structures (Vergés, 1993; Sans and Vergés, 1995). Folding by buckling preceded the main thrusts as it can be inferred by the fact that the main thrusts are not folded (Sans and Vergés, 1995). Layer parallel shortening was achieved prior to folding since all the strain ellipses in the XZ section have the same orientation after unfolding. Therefore, the sedimentary pile was shortened 16%-23 by layer parallel shortening and this mechanism was blocked before folding. Similar processes have also been documented in sand box models (Liu and Dixon, 1990; Mulugueta and Koyi, 1992; Koyi, 1995) and in other field examples (Averbuch et al., 1992, 1993; Casas et al., 1996; Mukul and Mitra, 1998).

## DIAPIRISM

The distinction between diapirs formed under horizontal stresses and those formed in “static” conditions has been addressed in several papers (Berkel, 1986; Talbot et al., 1988; Koyi, 1988). The plan shape of diapirs has been suggested to be diagnostic of diapirs formed under a tectonic contraction (Koyi, 1988). In this regard, elongated diapirs have usually been related with either pre- or syntectonic development, whereas circular diapirs have been

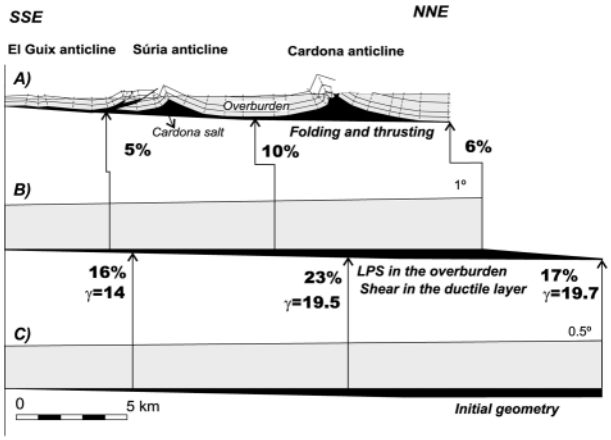


FIGURE 16 **Restoration of the salt basin to the pre-deformation scenario. A) Present day section. B) Restoration of the folding and thrusting preserving overburden bed length and basal dip of the salt layer. This restitution does not take into account the layer parallel shortening (LPS) calculated in this work. Shortening due to folding and thrusting ranges from 5% to 10% in the anticlines. The sedimentary dip of the top of the overburden is restored to 1º. C) Restoration taking into account shortening due to folding and thrusting and LPS. Overburden bed length and salt area are preserved. The sedimentary dip of the top of the overburden is restored to 0,5º and the basal dip of the salt layer has to be modified and evidences a tilt of 0.7º related to a Neogene extension.**

related to absence of horizontal stresses. Moreover, syncompressional diapirs have only been succesfully modelled by Vially et al. (1994), and Costa and Vendeville (1999), both in very specific scenarios. In the model by Vially et al. (1994) diapirs formed during shortening because a tear fault cut the folded overburden. This fault allowed the salt to rise and pierce the overburden. The most significant characteristic of the diapirs formed in this way is that they are elongated perpendicular to the fold axes. In the model by Costa and Vendeville (1999) a diapir formed in the hangingwall of a thrust when, as it is transported upwards, the thrust front at the surface collapses; creating an extensional situation which triggers diapirism of an irregular salt layer which is transported in the hangingwall. The diapirs resulting from this model form in a very specific situation of a local extension in a shortening regional setting and are elongated parallel to the fold axes.

In the South Pyrenean Triangle zone only the Cardona anticline has been pierced by a diapir (Marín and Rubio, 1914; Marín, 1923; Menéndez, 1923; Barandica et al., 1926; Ríos, 1959; Monturiol and Font Altaba, 1968; Riba, 1970; Iglesias, 1970; Pueyo 1970, 1975; Wagner et al., 1971; Pueyo and San Miguel, 1974; Riba et al., 1983; Pinto and Casas, 1996). The hinge of the Cardona anticline is well defined in the western and central parts of the anticline and becomes broader towards the east. The Cardona diapir is located close to the eastern termination of the anticline and marks the transition between the narrow and wide hinge zones. Where the diapir pierces the anticline, the total shortening in the anticline is 23% (Fig. 15). Folding accounts for 6% whereas 17% is accommodated by layer parallel shortening (Sans, 1999). The overburden in the diapir area consists of 100 m of grey marls at the bottom of the Barbastro Fm., 450 m of sandstones and marls from the Súria Fm. and 1500 m of sandstones and conglomerates from the Solsona Fm. that at the base of the unit are interbedded with thin limestones from the Castelltallat Fm. (Fig. 13). The preserved thicknesses are 400 m in the anticline crest, approximately 2000 m in the northern syncline trough and 1200 m in southern one. The contact between the overburden and the diapir corresponds to a 2-6 m thick external shear zone formed by a melange of country rock and sheared salt. Apart from this zone, no significant deformation is observed in the overburden units close to the diapir (Iglesias, 1970; Wagner et al., 1971; Riba et al., 1983). The diapir develops a 250-500 m wide and approximately 250 m high stem. The present day erosion reveals outward-verging folds, indicating the initiation of a bulb (Fig. 17). The structure of the salt layers, the complete stratigraphic sequence in a normal position and especially the horizontal fold axial planes in the highest parts of the diapir suggest that the bulb is almost completely preserved close to the diapir walls. The diapiric bulb is small, approximately 60-80 m high and 400 to 700 m wide, and around 2 km long, elongated parallel to the Cardona anticline axis. Its internal structure consists of a major anticline parallel to the Cardona anticline cut by a shear zone of the same trend (Sans, 1999). The fold axial planes and fold axes are vertical or highly dipping near the western and eastern terminations of the diapir whereas in the central part of the diapir the axial planes are vertical and the fold axes subhorizontal, and mainly with a NE-SW trend (Wagner et al., 1971; Sans, 1999). This, together with the cross cutting relationships between boudins and fold axes which are parallel to each other in the center of the diapir and perpendicular in both terminations (Sans, 1999), suggest that the folds are large sheath folds elongated in a NE-SW direction (Fig. 18). The significance of the shear zone cutting the main salt anticline, and dividing the diapir into two can be compared to that of the internal shear zones of Kupfer (1968, 1976) and could indicate different rates of salt movement between both sides of the shear zone. In this regard two main spines in the Cardona diapir could be defined. The southeastern spine has relatively reached higher levels than the northwestern one.

The onset of the Cardona diapir cannot be well constrained from the geometrical relationships with the surrounding sediments. The oldest record of movement of the diapir corresponds to the drag that the post-Oligocene poorly consolidated sandstones show around the diapir (Fig. 17). The age of these sediments has been attributed

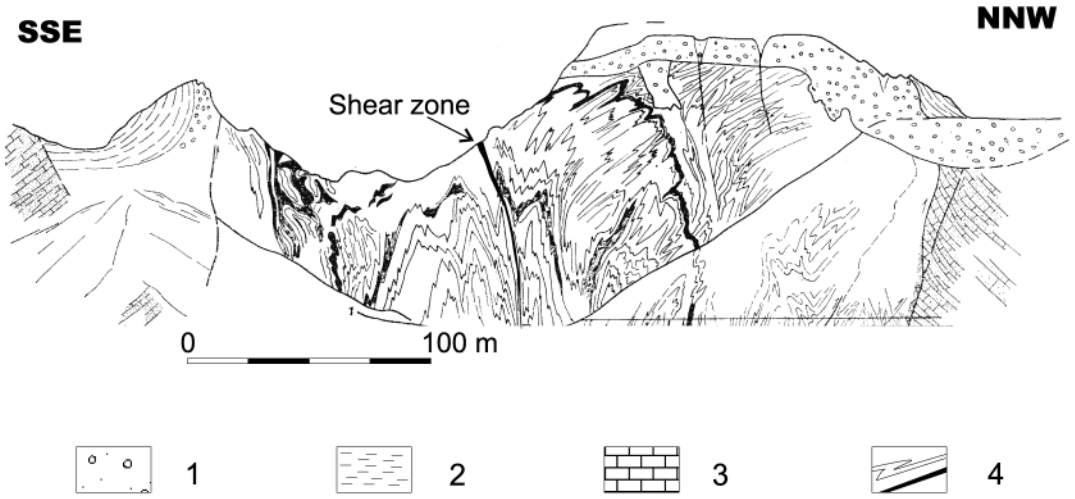


FIGURE 17 **Field drawing of the Cardona diapir in the called "Muntanya de sal". Modified from Wagner et al. (1971). 1: caprock; 2: Plio-Quaternary sediments; 3: Oligocene; 4: Cardona Fm. The shear zone which separates the two spines is indicated in black.**

to middle Villafranquian (Riba, 1975), based on its correlation with a river terrace containing an association of fauna with *Elephas meridionalis* (Solé-Sabarís and Masachs, 1940; Masachs, 1952). Villafranquian period which was defined by Bonifany (1975) comprises the modern Plasencian and Calabrian times (Riba and Reguant, 1986). The middle Villafranquian ranges between 0.9-1.7 Ma. These sediments flexure upward from horizontal, 25 m away from the diapir, to subvertical close to it. The difference in height between the horizontal part and the highest point of a single layer indicates the minimum rise of the salt since deposition of the layer (compaction is estimated to be very little).

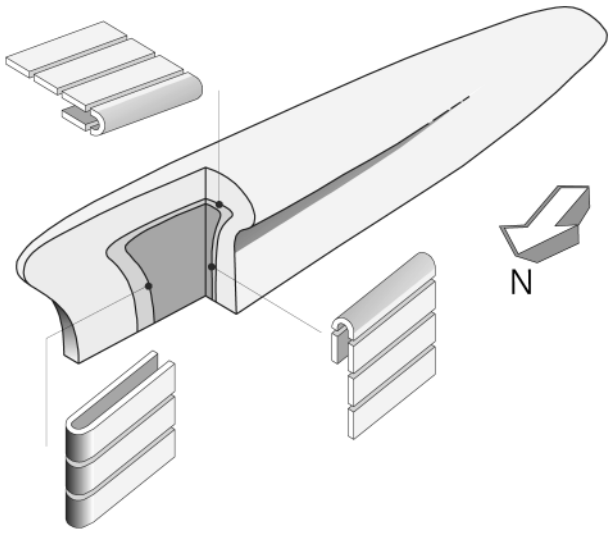


FIGURE 18 **Sketch of the geometry of the Cardona diapir (not to scale). The stratigraphic sequence is always in a normal position and the higher parts are located to the northeast, close to the Cardener river. The relationship between boudins and folds suggest that the structure mainly consists of large sheath folds elongated in a NE-SW direction. Dark gray represents the lower massive salt member, the lighter gray the potassium salt levels and the lightest gray the upper salt member (halite and carnalite).**

Present upward movement of the diapir is evidenced by the presence of salt at surface giving a local relief in the present climatic conditions. The Cardona diapir crops out in a subordinate valley, which drains to the Cardener river and only in the western part of the valley, the Cardona salt is exposed 100 m above the valley floor giving a local topographic relief of 100 m ("Muntanya de sal"). This relief is around 50 m to 100 m lower than the highest surrounding topography. The presence of this relative relief in a climatic regime dominated by dissolution suggests that the diapir is still active. The upward movement of the diapir is also supported by topographic measurements carried out in the period 1979-1986. These measurements indicate that, away from the influence of the underground mining galleries in the deeper levels of the diapir and the salt cored anticline, the leveling points have an average upward vertical motion of 1 mm $yr^{-1}$ (Cardona, Internal Report).

However, none of this information determines the piercing age of the diapir. A pre-shortening age can be ruled out because the Cardona salt is younger than the initiation of shortening (Oligocene). Therefore only a syn- or post-compressional age are possible. Field evidences indicate a deep erosion in the Ebro basin during late Tertiary and Quaternary times. This event is suggested, in this work, to be the key factor to trigger diapirism (Sans, 1999; Sans and Koyi, 2001). A centrifuge model was prepared to simulate a phase of shortening and a phase of deep erosion

like that in the South Pyrenean foreland basin (Fig. 19). The model was, initially, 7.2 cm wide, 12 cm long and 1.8 cm thick. It was shortened (up to 12%) until the geometry of the folds was similar to the Cardona anticline, and the ductile layer accumulation in the anticline core was 3 times the initial source layer thickness. The amount of erosion in the model was also similar to the present day erosion in the crest of the Cardona diapir.

At 12% shortening in the centrifuge the model developed 6 symmetric buckle folds (Fig. 19B). The wavelength of the folds ranged between 1.5 and 2.3 cm and their amplitude between 3.5 and 5 mm. The wavelength/amplitude ratio in these anticlines was ranging between 4/1 to 7.6/1. The limbs of the folds dip 30º-40º and were characterized by round hinges. At the salt/overburden interface synclines and anticlines had similar size. At the surface of the model, anticlines were much wider than the synclines. The folds were rectilinear in trend and extended across the whole model.

After erosion (Fig. 19C), diapirs rose due to differential loading that forced the ductile layer to flow from underneath the area with higher overburden load (under the synclines) to the areas with less loading (the cores of anticlines). During growth of the diapirs, the geometry of the anticlines was modified. The anticlines became slightly asymmetric and the dip of their limbs increased to 40º-50º. In plan view, all the diapirs were elongate parallel to the fold axes and pierced the anticlines in the hinge area. However, in some asymmetric anticlines, the diapirs had oblique stems and pierced the back limb of the anticlines close to the crest. The diapirs had short stems and small bulbs (central diapir in Fig. 19D). When they reached the surface, they spread asymmetrically in the direction of the anticline vergence and their neck widened (side diapir in Fig. 19D).

The geometrical features of the diapir such as having elongated plan views parallel to the fold trend, piercing close to the hinge of the anticline, having a short and narrow neck and a small bulb, together with the documented deep erosion in the Ebro basin (Coney et al., 1996; Vergés et al., 1998) suggest that the Cardona diapir could have a similar evolutionary history to the model diapirs. The Cardona diapir, would have formed in a post-shortening setting and the age of the diapir can be estimated by the calculation of the piercing thickness. A first estimate to do this was done by balancing the forces acting against and in favor of piercing (Sans and Koyi, 2001). The result of this approximation gives an age for the Cardona diapir of around 2 My.

Erosion increases the differential loading on the salt layer and weakens the overburden, and therefore promotes diapirism without any need of changing the tecton-

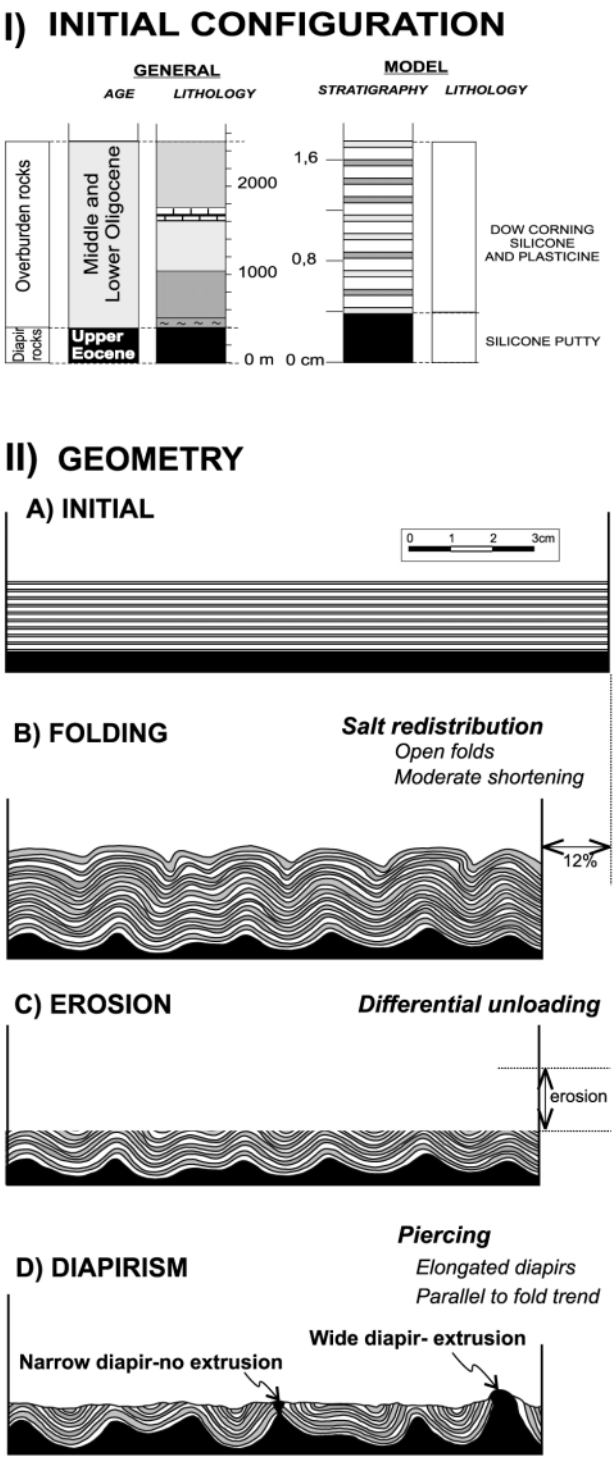


FIGURE 19 **I: Initial configuration of the model. Right column corresponds to the overburden in the Cardona diapir, left column to the model materials. II: Geometry of the main stages of the model. A) Initial configuration. B) After 12% folding the geometry of the anticlines is similar to the Cardona anticline. C) Erosion of the model. D) Development of diapirs. The geometry of the diapir in the center of the model is very similar to the Cardona diapir, short neck and small bulb before extrusion.**

ic regime. In a previously compressed area, two conditions have to be accomplished to create a diapir as illustrated in the model. First, the folds have to be open structures (Fig. 19B) and second, deep erosion has to take place (Fig. 19C). Compression inhibits diapirism by thickening the overburden, but it also redistributes the salt layer by accumulating it in the core of the anticlines where its thickness can be several times larger than in the initial source layer. Moderate amount of shortening in the external areas of fold-and-thrust belts does not expel the salt back to the salt layer from the anticline cores (Wilschko and Chapple, 1977). This results in a larger salt/overburden thickness ratio under the anticline crest than in the pre-shortening stage. After this differential accumulation of the salt layer, erosion thins the overburden, especially on the anticline crests, where the salt/overburden thickness ratio is larger. The resulting differential loading between the synclinal trough and the anticline crest promotes salt flow towards the areas of lower pressure. Piercing takes place when the critical overburden thickness is reached. The diapirs formed in this way are expected to be elongate parallel to the fold trend. They pierce the hinge of the anticlines or in the back limb of asymmetric anticlines close to the hinge. In section, the diapirs have short and narrow necks and small bulbs that widen as they extrude at the surface. During this process the geometry of the anticlines that are being pierce is modified, the dip of their limbs increases and the salt area in the core is reduced.

## CONCLUSIONS

Triangle zones form where the basal decollement of a fold and thrust belt meets a ductile detachment level. The preservation in the South Pyrenees of several subsequent triangle zones suggests that they form at different stages of the evolution of a fold-and-thrust belt and not only in the last stage of deformation. Their preservation during orogenic development is conditioned by the further displacement of the basal detachment. Moreover, where the ductile detachment consists of salt, triangle zones form continuously during the development of the fold-and-thrust belt at the deformation front. In contrast, where the ductile detachment consists of gypsum, the triangle zones form only at the pinch-out of the ductile layer.

The thickness and shape of the ductile detachment greatly influence the geometry of the folds developed above it. On the other hand, the variation in the pinch-out orientation of the ductile layer may lead to the almost synchronous development of different fold trends. On the other hand, the decrease in the salt thickness due, for example, to a basal slope in the salt layer, changes the shape of the anticlines at depth. Anticlines change from salt cored detachment anticlines where the salt is thick enough to fill the core of the anticlines to anticlines cored by a synclinal antiformal-root where it is not thick enough. Recognition of such structures is of fundamental importance to economically evaluate mining and oil prospects.

External areas of fold-and-thrust belts detached above salt can reach values of internal distortion that can be several times greater than the shortening achieved by folding and thrusting. This internal distortion of the overburden is recorded in the salt horizon as a generalized shear event. Moreover, this internal distortion should be taken into account during section restoration, and especially if restoring the salt basin and the overburden.

Erosion alone may trigger diapirism in areas where salt has accumulated in the anticline cores due to differential unloading. Diapirs triggered by this unroofing mechanism are elongated parallel to the fold axes, have short stems and small bulbs before extruding at the surface. These results warn against identification of syn-shortening diapirs by their horizontal elliptical section alone. Application of this concept to the eastern south-Pyrenean folds suggested an age of 2 Ma for the Cardona diapir, and a future piercing for the rest of the anticlines.

The eastern South Pyrenean front has undergone a wide range of phenomena, from thrust tectonics to diapirism. Shortening in the first stages of deformation resulted in layer parallel shortening of up to 20% in the sediments located 500 m above the detachment, and in a generalized top-to-the-foreland shear in the salt layer. Further shortening folded the overburden and salt flowed into the cores of the anticlines. Where the salt layer was thin and the basal slope was high, anticlines cored by synclinal antiformal-roots formed, whereas where the salt layer was thicker south-directed detachment anticlines formed. Amplification of the anticlines was accompanied by the subsidence of the synclines into the ductile layer. The reduction of the salt layer under the synclines and the increase in basal friction resulted in thrusting of the folds. After folding, differential erosional unloading between the anticline and syncline crests provided the differential loading needed to trigger diapirism in the crestal areas of the anticlines, which have reached the critical piercing thickness.

## ACKNOWLEDGMENTS

I would like to thank P. Santanach for his supervision, and J. Vergés and H. Koyi for their help in many of the subjects included in this summary.

## REFERENCES


Agustí, J., Anadón, P., Arbiol, S., Cabrera, L., Colombo, F., Sáez, A., 1987. Biostratigraphical characteristics of the Oligocene sequences of North-Eastern Spain (Ebro and Campins Basins). Münchner Geowissenschaftliche Abhandlungen, A10, 35-42.

Anadón, P., Cabrera, L., Colldeforns, B., Sáez, A., 1989. Los sistemas lacustres del Eoceno superior y Oligoceno del sector oriental de la cuenca del Ebro. Acta Geologica Hispanica, 24, 205-231.

Ayora, C., Taberner, C., Pierre, C., Pueyo, J.J., 1995. Modelling the sulphur and oxygen isotopic composition of sulphates through a halite-potash sequence: Implications for the hydrological evolution of Upper Eocene Southpyrenean Basin. Geochimica et Cosmochimica Acta, 59, 1799-1808.

Auverbuch, O., Frizon de Lamotte, D., Kissel, C., 1992. Magnetic fabric as a structural indicator of the deformation path within a fold-thrust structure: a test case from the Corbieres (NE Pyrenees, France). Journal of Structural Geology, 14, 461-474.

Auverbuch, O., Frizon de Lamotte, D., Kissel, C., 1993. Strain distribution above a lateral culmination: an analysis using microfaults and magnetic fabric measurements in the Corbieres (NE Pyrenees, France). Annales Tectonicae, VII, 3-21.

Barandica, M., García Siñeriz, J., Milans del Bosch, J., Gil, R., Sans Huelin, G., 1926. Investigaciones geofísicas de la cuenca potásica de Cataluña. Boletín del Instituto Geológico y Minero de España , 47, 351-380.

Berkel, J.T., 1986. A structural study of evaporite diapirs, fold and faults, Axel Hiberg Island, Canadian Artic Islands. Amsterdam, GUA Papers of Geology, Series 1, 26, 149 pp.

Bonifany, E., 1975. L'Ere quaternaire. Bulletin de la Société Géologique de France, 17, 380-393.

Braunstein, J., O'Brien, G.D. (eds.), 1968. Diapirism and Diapirs. Tulsa, American Association of Petroleum Geologists Memoir, 8, 444 pp.

Burbank, D. W., Puigdefábregas, C., Muñoz, J.A., 1992a. The chronology of the Eocene tectonic and stratigraphic development of the eastern Pyrenean basin, NE Spain. Geological Society of America Bulletin, 104, 1101-1120.

Burbank, D.W., Vergés, J., Muñoz, J.A., Benthan, P.A., 1992b. Coeval hindward and forward imbricating thrusting in the central southern Pyrenees, Spain: timing and rates of shortening and deformation. Geological Society of America Bulletin, 104, 3-17.

Busquets, P., Ortí, F., Pueyo, J.J., Riba, O., Rosell, L., Sáez, A., Salas, R., Taberner, C., 1985. Evaporite deposition and diagenesis in the saline (potash) Catalan Basin, Upper Eocene. In: Milá, D., Rosell, J. (eds.). 6th European Regional Geology Meeting (IAS), Excursion Guidebook, Lleida, Spain, 13-59.

Casas, J.M., Durney D., Ferret J., Muñoz J.A., 1996. Determinación de la deformación finita en la vertiente sur del Pirineo oriental a lo largo de la transversal del río Ter. Geogaceta, 20(4), 803-805.

Cobbold, P.R. (ed.), 1993. New insights into salt tectonics. Tectonophysics, 228(3-4), 445 pp.

Coney, P., Muñoz, J.A., McClay, K.R, Evenchick, C.A., 1996. Syntectonic burial and post-tectonic exhumation of the southern Pyrenees foreland fold-thrust belt. Journal of the Geological Society, 153, 9-16.

Costa, E., Vendeville, B., 1999. Style and kinematics of folding and diapirism in experimental model of shortening above a viscous decollement. London, Thrust Tectonics Conference, Abstract with Program, 161-162.

Cousenz, B.A., Wiltchsko, D.V., 1996. The control of mechanical stratigraphy on the formation of triangle zones. Canadian Petroleum Geology Bulletin, 44(2), 165-179.

Dalhstrom, C.D.A., 1990. Geometric constraints derived from the law of conservation of volume and applied to evolutionary models for detachment folding. American Association of Petroleum Geologists Bulletin, 74, 336-344.

Davis, D.M., Engelder, T., 1985. The role of salt in fold-and-thrust belts. Tectonophysics, 119, 67-88.

Davison, I., Alsop, G.I., Blundell, D.J. (eds.), 1996. Salt Tectonics. Geological Society Special Publication, 100, 310 pp.

Epard, J.L., Groshong, R.H., 1993. Excess area and depth to detachment. American Association of Petroleum Geologists Bulletin, 77, 1291-1302.

Fontboté, J.M., Muñoz, J.A., Santanach, P., 1986. On the consistency of proposed models for the Pyrenees with the structure of the eastern parts of the belt. Tectonophysics, 129, 291-301.

Gil, J., Jurado, M.J., 1998. Geological interpretation and numerical modelling of salt movement in the Barbastro-Balaguer anticline, southern Pyrenees. Tectonophysics, 293(3-4), 141-155.

Gordy, P.L., Frey, F.R., Norris, D.K., 1977. Geological Guide for the CSPG 1977 Waterton-Glacier Park Field Conference. Calgary, Canadian Society of Petroleum Geologists, 93 pp.

Groshong, R.H., Epard, J.L., 1994. The role of strain in area-constant detachment folding. Journal of Structural Geology, 16, 613-618.

Hardy, S., Poblet, J., 1994. Geometric and numerical model of progressive limb rotation detachment folds. Geology, 22, 371-374.

Harrison, J.C., Bally, A.W., 1988. Cross-section of the Parry Island fold belt on Melville Island, Canadian Artic Islands: implications for the timing and kinematic history of some thin-skinned decollement systems. Canadian Petroleum Geology Bulletin, 36, 311-332.

Harrison, J.C., 1991. Melville Island's salt-based fold belt (Arctic Canada). Doctoral thesis. Rice University, Houston, 449 pp.

Hatcher, R., 1999. Development of triangle zones in the Evolution of Foreland Fold-Thrust belts. American Association of Petroleum Geologists Annual convention. San Antonio, A56.

Homza, T.X., Wallace, W.K., 1995. Geometric and kinematic models for detachment folds with fixed and variable detachment depths. Journal of Structural Geology, 17(4), 575-588.

Iglesias, M., 1970. Estudio estratigráfico y tectónico del área de

Súria-Cardona. Master thesis. Universitat de Barcelona, 77 pp.

Jackson, M.P.A., Talbot, C. J., 1991. A glossary of salt tectonics. Geological circular, 91(4). Bureau of Economic Geology, University of Texas at Austin, 41 pp.

Jackson, M.P.A., Vendeville, B., 1994. Regional extension as a geologic trigger for diapirism. Geological Society of America Bulletin, 106, 57-73.

Jackson, M. P. A., Roberts, G., Snelson, S. (eds.), 1995. Salt tectonics a global perspective. American Association of Petroleum Geologists Memoir, 65, 454 pp.

Jenyon, M.K, 1986. Salt Tectonics. London, Elsevier Applied Science, 191 pp.

Jordan, P., Nuesch, R., 1989. Deformation structure in the Mushelkalk anhidrites of the Schafirsheim (Jura overthrust, Northern Switzerland). Eclogae Geologicae Helveticae, 82, 429-454.

Koyi, H., 1988. Experimental Modeling of Role of Gravity and lateral shortening in Zagros mountain belt. American Association of Petroleum Geologists Bulletin, 72(11), 1381-1394.

Koyi, H., 1995. Mode of internal deformation in sand wedges. Journal of Structural Geology, 17(2), 293-300.

Kupfer, D.H., 1968. Relationship of internal to external structure of salt domes. In: Braunstein, J., O'Brien, G.D. (eds.). Diapirism and Diapirs. American Association of Petroleum Geologists Memoir, 8, 79-89.

Kupfer, D.H., 1976. Shear zones inside gulf coast stocks help to delineate spines of movement. American Association of Petroleum Geologists Bulletin, 60, 1434-1447.

Lerche, I., O'Brien, J.J., 1987. Dynamical Geology of salt and related structure. London, Academic Press, 830 pp.

Letouzey, J., Coletta, B., Vially, R., Chermette, J.C., 1995. Evolution of salt-related structures in compressional settings. In: Jackson, M.P.A., Roberts, G., Snelson, S. (eds.). Salt tectonics a global perspective. American Association of Petroleum Geologists Memoir, 65, 41-60.

Liu, S., Dixon, M., 1990. Centrifuge modeling of thrust faulting: strain partitioning and sequence of thrusting in duplex structures. In: Knipe, R.J., Rutter, E.H. (eds.). Deformation Mechanisms, Rheology and Tectonics. Geological Society Special Publication, 54, 431-444.

MacKay, P.A., Vasek, J.L., Kubli, T.E., Dechesne, R.G., Newson, A.C., Reid, J.P., 1996. Triangle Zones and Tectonic wedges. Canadian Petroleum Geology Bulletin, 44, 428 pp.

Malavielle, J., Ritz, J. F., 1989. Mylonitic deformation of evaporites in décollements: examples from the southern Alps, France. Journal of Structural Geology, 11, 583-590.

Marcoux, J., Brun, J.P., Burg, J.P., Ricou, L.E., 1987. Shear structure in anhydrite at the base of thrust sheets (Antalya, Southern Turkey). Journal of Structural Geology, 9, 555-561.

Marín, A., Rubio, C., 1914. Sales potásicas de Cataluña. Boletín del Instituto Geológico y Minero de España, 34, 173-230.

Marín, A., 1923. Investigaciones de la cuenca potásica de Cataluña. Boletín del Instituto Geológico y Minero de España, 64, 3-78.

Masachs, V., 1952. La edad y origen de los movimientos de las sales paleógenas de la cuenca del Ebro. Memoria y Comunicaciones del Instituto Geológico de Barcelona, IX, 51-65.

Meigs, A., Vergés, J., Burbank, D.W., 1996. Ten-million-year history of a thrust sheet. Geological Society of America Bulletin, 108(12), 1608-1625.

Menéndez, L., 1923. Trabajos en investigaciones de laboratorio referentes a las sales potásicas de Cataluña. Boletín del Instituto Geológico y Minero de España, 64, 79-99.

Miralles, L., Sans, M., Galí, S., Santanach, P., 2001. 3-D Rock salt fabric in a shear zone (Súria anticline, South-Pyrenees). Journal of Structural Geology, 23, 675-691.

Monturiol, J., Font Altaba, M., 1968. Sobre la movilidad de la halita, la silvinita y las arcillas durante las deformaciones tectónicas. Acta Geologica Hispanica, 3(4), 108-110.

Mukul, M. G., Mitra, S., 1998. Finite strain variation analysis in the sheeprock thrust sheet: an internal thrust sheet in the Proto salient of the Serier fold-and-thrust belt. Central Utah. Journal of Structural Geology, 20, 385-405.

Mulugueta, G., Koyi, H., 1992. Episodic accretion and strain partitioning in a model sand wedge. Tectonophysics, 202, 319-333.

Muñoz, J.A., Martínez, A., Vergés, J., 1986. Thrust sequences in the eastern Spanish Pyrenees. Journal of Structural Geology, 8, 399-405.

Muñoz, J.A., 1992. Evolution of a continental collision belt: ECORS-Pyrenees crustal balanced cross-section. In: McClay, K. (ed.). Thrust tectonics. London, Chapman and Hall, 235-246.

Pardo, G., Villena, J., 1979. Aportación a la geología de la región de Barbastro. Acta Geologica Hispanica, 14, 289-292.

Pinto, V., Casas, A., 1996. An interactive 2D and 3D gravity modeling program for IBM-Compatible personal computers. Computers and Geosciences, 22, 535-546.

Poblet J., McClay, K., 1996. Geometry and kinematics of single-layer detachment folds. American Association of Petroleum Geologists Bulletin, 80(7), 1085-1109.

Pueyo, J.J., 1970. Estudio geológico de los yacimientos salinos de Sallent y Balsareny. Master thesis. Universitat de Barcelona, 72 pp.

Pueyo, J.J., 1975. Estudio petrológico y geoquímico de los yacimientos potásicos de Cardona, Súria, Sallent (Barcelona, España). Doctoral thesis. Universitat de Barcelona, 351 pp.

Pueyo, J.J., San Miguel, A. 1974. Características petrológicas de las sales sódicas, potásicas y magnésicas de la cuenca potásica Catalana. Institut d'Investigacions Geològiques de la Diputació Provincial de Barcelona, 29, 23-49.

Puigdefàbregas, C., Muñoz, J.A., Marzo, M., 1986. Thrust belt development in the Eastern Pyrenees and related depositional sequences in the southern foreland basin. In: Allen, Ph., Homewood, P. (eds.). Foreland Basins. Special Publication of the International Association of Sedimentologists, 8, 229-246.

Riba, O., 1970. Informe geológico sobre el área de Cardona. CGS Internal Report, 52 pp.

Riba, O., 1975. Mapa Geologico de España. Scale 1:50.000, 2nd. series, no. 330, Cardona. Madrid, Instituto Geológico y

Minero de España, Serv. Publ., Ministerio Industria, 58 pp., 1 fold map.

Riba, O., Reguant, S., Villena, X., 1983. Ensayo de síntesis estratigráfica y evolutiva de la cuenca terciaria del Ebro. In: Libro Jubilar J.M. Ríos. Geología de España II, Madrid, Instituto Geológico y Minero de España, 131-159.

Riba, O., Reguant, S., 1986. Una taula dels temps geològics. Barcelona, Institut d'Estudis Catalans, Arxius de la secció de ciències LXXXI, 127 pp.

Richter-Bernburg, G., 1980. Interior structures of salt bodies. Bulletin des Centres de Recherches, Exploration-Production Elf-Aquitaine, 4, 373-393.

Ríos, J.M., 1959. Materiales salinos del suelo español. Memorias y Comunicaciones del Instituto Geológico y Minero de España, 64, 166 pp.

Rosell, L., Pueyo, J.J., 1997. Second marine evaporitic phase in the South Pyrenean foredeep: The Priabonian Potash Basin. In: Busson, G., Schreiber, B. Ch. (eds.). Sedimentary deposition in rift and foreland basins in France and Spain (Paleogene and Lower Neogene). New York, Columbia University Press, 358-387.

Sáez, A., 1987. Estratigrafía y sedimentología de las formaciones lacustres del tránsito Eoceno Oligoceno del NE de la cuenca del Ebro. Doctoral thesis. Universitat de Barcelona. 353 pp.

Sáez, A., Riba, O., 1986. Depósitos aluviales y lacustres paleógenos del margen pirenaico central y cuenca del Ebro. Libro guia Exc. XI Congreso Español de Sedimentología, Barcelona, 6.1-6.29.

Sans, M., Vergés, J., 1995. Fold development related to contrational salt tectonics: southern Pyrenean thrust front, Spain. In: Jackson, M.P.A., Roberts, G., Snelson, S. (eds.). Salt tectonics a global perspective. American Association of Petroleum Geologists Memoir, 65, 369-378.

Sans, M., Muñoz, J.A., Vergés, J., 1996a. Triangle zone and thrust wedge geometries related to evaporitic horizons (southern Pyrenees). Canadian Petroleum Geology Bulletin, 44(2), 375-384.

Sans, M., Sánchez, A., Santanach, P., 1996b. Internal structure of a detachment horizon in the most external part of the Pyrenean fold and thrust belt (northern Spain). In: Alsop, G.I., Davison, I. (eds.). Salt Tectonics. Geological Society Special Publication, 100, 65-76.

Sans, M., 1999. From thrust tectonics to diapirism: the role of evaporites in the kinematic evolution of the Eastern South-Pyrenean front. Doctoral thesis. Universitat de Barcelona, 197 pp.

Sans M., Koyi, H., 2001. Modeling the role of erosion in diapir development. In: Koyi, H.A., Mancktelow, N.S. (eds.). Tectonic Modelling: A Volume in Honor of Hans Ramberg. Geological Society of America Memoir, 193, 111-122.

Senz, J.G., Zamorano, M., 1992. Evolución tectónica y sedimentaria durante el Priaboniense superior-Mioceno inferior en el frente de cabalgamientos de las sierras Marginales Occidentales. Acta Geologica Hispanica, 27, 195-209.

Solé-Sabarís, L., Masachs, V., 1940. Edad de las terrazas del río Cardoner en Manresa. VI. Estudios Geomorfológicos de la Península Ibérica, 2, 3-6.

Talbot, C.J., Jackson M.P.A., 1987. Internal kinematics of salt diapirs. American Association of Petroleum Geologists Bulletin, 71, 1068-1093.

Talbot, C.J., Koyi, H., Sokoutis, D., Mulugeta, G., 1988. Identification of evaporite diapirs formed under the influence of horizontal compression: a discussion. Canadian Petroleum Geology Bulletin, 36(1), 91-95.

Vendeville, B.C., Mart, Y., Vigneresse, J.L. (eds.), 2000. Salt, shale and igneous diapiris in and around Europe. London, Geological Society Special Publication, 174, 207 pp.

Vergés, J., Muñoz, J.A., Martínez, A., 1992. South Pyrenean fold-and-thrust belt: role of foreland evaporitic levels in thrust geometry. In: McClay, K. (ed.). Thrust tectonics. London, Chapman and Hall, 255-264.

Vergés, J., 1993. Estudi geològic del vessant sud del Pirineu Oriental i Central. Evolució cinemàtica en 3D. Doctoral thesis. Universitat de Barcelona, 200 pp.

Vergés, J., Millán, H., Roca, E., Muñoz, J.A., Marzo, M., Cirés, J., Den Bezemer, T., Zoetemijer, R., Cloetingh, S., 1995. Eastern Pyrenees and related foreland basins: pre-, syn, and post-collisional crustal-scale cross-sections. Marine and Petroleum Geology, 12(8), 893-915.

Vergés, J., Marzo, M., Santaularia, T., Serra-Kiel, J., Burbank, D.W., Muñoz, J.A., Gimenez-Montsant, J., 1998. Quantified vertical motions and tectonic evolution of the SE Pyrenean foreland basin. In: Mascle, A., Puigdefàbregas, C., Lutherbacher, H.P., Fernández, M. (eds.). Cenozoic Foreland Basins of Western Europe. Geological Society Special Publication, 134, 107-134.

Vially, R., Letouzey, J., Bernard, F., Haddadi, N., Deforges, G., Askri, H., Boudjema, A., 1994. Basin inversion along the North African Margin. The Sahara Atlas (Algeria). In: Roure, F. (ed.). Tethyan Platforms. Paris, Technip, 79-118.

Wagner, G., Mauthe, F., Mensik, H., 1971. Der Salztock von Cardona in Nordostpanien. Geologische Rundschau, 60, 970-996.

Wiltschko, D.V., Chapple, W.M., 1977. Flow of weak rocks in Appalachian Plateau folds. American Association of Petroleum Geologists Bulletin, 61, 653-670.

**Manuscript received September 2001;**
**revision accepted May 2002.**